Fabrication of ultra-high working range strain sensor using carboxyl CNTs coated electrospun TPU assisted with dopamine

Yuhao Wang [1], Wenyue Li [1], Chenchen Li [1], Bangze Zhou [1], Yanfen Zhou [1], Liang Jiang [1, *], Shipeng Wen [2], Fenglei Zhou [1, 3, *]

[1] College of Textiles and Clothing, Qingdao University, Qingdao, 266071, China

[2] Beijing Engineering Research Center of Advanced Elastomers, Beijing University of Chemical Technology, Beijing 100029, China

[3] Department of Medical Physics and Biomedical Engineering, University College London, London, WC1V 6LJ, UK

Abstract

Fiber-based strain sensors have attracted widespread concern of researchers due to large specific surface area, good stretchability and remarkable flexibility. In this work, a stretchable strain sensor with ultra-high working range was developed by using electrospun thermal plastic polyurethane (TPU) nanofibrous membrane coated with carboxyl multi-walled carbon nanotubes (CNTs). In order to obtain an even distribution and an improved fastness of carboxyl CNTs on TPU fibers, dopamine (DA) was employed to modify the TPU nanofibrous membrane (labelled DATPU) via a fast ultrasonication-assisted deposition approach. DATPU/CNTs exhibited an ultra-high working range of about 710% with high gauge factor up to 1200. Furthermore, DATPU/CNTs were found to have stronger washing fastness than TPU/CNTs owing to the introduction of DA onto the surface of TPU nanofibers. DATPU/CNTs also maintained good electrical conductivity during 15000 cycles of stretching-releasing test.

[*] Corresponding authors, email address: liang.jiang@qdu.edu.cn, fenglei.zhou@ucl.ac.uk

Finally, a prototype of strain sensor based on DATPU/CNTs membrane demonstrated remarkable flexibility and sensitivity to human body motions such as elbow bending, finger bending and swallowing.

Keywords: Polyurethane nanofibers; electrospinning; dopamine modification; carbon nanotubes; strain sensor

Introduction

Recently, the demand of smart wearable electronics with the advantages of intelligence, compact size and portability has soared sharply [1-3], because they could provide great potential in human motion detection and health monitoring, etc [4-7]. One important category is strain sensors, which possess the ability of transforming the physical deformation into electrical signals [8]. An excellent strain sensor should have a wide working range, high sensitivity and good durability [9-11]. However, conventional metal-based and semiconductor-based strain sensors are subject to the stiffness, poor working range (< 5%) and low sensitivity, and therefore cannot meet the requirement of wearable device [12, 13].

Flexible strain sensors based on electrically conductive polymer fiber composites, which are composed of stretchable polymer fibers and conductive fillers or conductive layers, have been the focus of an increasing number of scientific publications because of its lightness, flexibility and stretchability [14, 15]. Stretchable polymer fibers elastomers, such as thermoplastic polyurethane (TPU) [16, 17], Ecoflex [18] and styrene butadiene styrene (SBS) [19], are generally fabricated by wet spinning [20], melt spinning [21] and electrospinning, etc. Among these, electrospinning as a simple and easy approach is usually utilized to manufacture micro/nano fibrous membrane, which possesses superiorities of large specific surface area and commendable mechanical flexibility [22]. Flexible strain sensors prepared by coating electrospun

fibrous membranes with carbon black (CB) [23], reduced graphene oxide (RGO) [24] and carbon nanotubes (CNTs) [25] have attracted increasing attention. For example, Zhao [9] et al. prepared a strain sensor by depositing CB particles onto electrospun TPU fibrous membrane assisted by ultrasonication. In order to improve the working stability of strain sensor, CB/TPU membrane was encapsulated into Ecoflex layer. The obtained CB/TPU/Ecoflex strain sensor exhibited an ultrahigh sensitivity, (i.e. the maximum gauge factor was up to 3186.4 at strain of 225%) while the working range was low (225%). In addition, Lu [26] et al. fabricated a silver nanowires (AgNWs)/TPU/polydimethylsiloxane (PDMS) sandwich structured strain sensor via sequential coating the electrospun TPU membrane with AgNWs and PDMS by filtration. The resultant strain sensor presented good stability and reliability, but was subject to low working range (about 80%) and low sensitivity (gauge factor, which refers to the sensitivity of conductive fibrous membranes to tension, was about 12). Gong [27] et al. incorporated the electrospun carbon sponge (CS) into PDMS to obtain a flexible and wearable strain sensor, which showed high piezoresistive sensibility and high-speed response. However, the working range and gauge factor (GF) of CS/PDMS strain senor was just up to 60% and 130.5, respectively. As pointed out in previous studies [28-31], a high working range could result in the reduction of materials service life in detecting high strain levels movement. Hence, there is a high-demand of electrospun fibrous membrane-based strain sensors with improved working range.

In this work, TPU electrospun fibrous membrane with excellent elasticity and toughness was selected as substrate. CNTs were selected as the conductive medium because of its very high mechanical strength and electrical conductivity. A highly stretchable strain sensor was fabricated by coating CNTs on TPU fibrous membrane assisted by ultrasonication. In order to further improve the electrical stability of the

membrane and the fastness of CNTs coated on the membrane, dopamine (DA), which was widely used to modify the surface of materials to improve the interfacial strength [32], was utilized to modify the TPU fibrous membrane (DATPU) to enhance the interfacial interactions between CNTs and TPU membrane. The influence of DA modification and the concentration of the CNTs suspension on the performance of conductive fibrous membrane were investigated. The ability of an optimized conductive fibrous membrane to detect various human body motions, such as swallow, finger bending, wrist bending and knee bending, was evaluated. Finally, a prototype strain sensor was assembled together with Bluetooth device and battery and its performance was demonstrated via detecting human kneecap motions.

Experimentation

Materials

TPU was acquired from Shandong INOV New Materials Co., Ltd. (Zibo, Shandong, China). CNTs were purchased from Cnano Technology (Beijing China). Tetrahydrofuran (THF), N, N-dimethylformamide (DMF) were bought from Sinopharm Chemical Reagent Co., Ltd. (Shanghai, China). Dopamine hydrochloride (DA·HCl) and Sodium periodate ($NaIO_4$) were obtained from Shanghai Macklin Biochemical Co., Ltd. (Shanghai, China). Tris (hydroxymethyl) aminomethane (Tris) was produced from Beijing Solarbio Science & Technology Co., Ltd. (Beijing, China). .

Preparation of electrospun TPU fibrous membrane

Figure 1(a) shows the procedure for fabricating electrospun TPU nanofibers. TPU pellets were initially desiccated in a vacuum oven at 80 °C for 24 h. Then, they were dissolved with concentration of 18 wt% in a mixed solvent of THF and DMF with a volume ratio of 3:1. The mixture was magnetically stirred at 60 °C for 8 h for complete dissolving. In order to obtain electrospun TPU fibrous membrane, TPU solution was

loaded in a plastic syringe (10 mL) connected to a 22-gauge blunt end needle which was fixed on a digital syringe pump (Longer Precision Pump Co., Ltd., Baoding, Hebei, China). Electrospinning was carried out under the room temperature, humidity of 25%, the applied voltage of 20 kV, the work distance of 20 cm between the capillary tip and the collector, and the solution supply rate of 4 mL/h. Finally, the resultant TPU fibrous membranes were placed in a fume hood overnight at room temperature to remove the remaining solvent as much as possible.

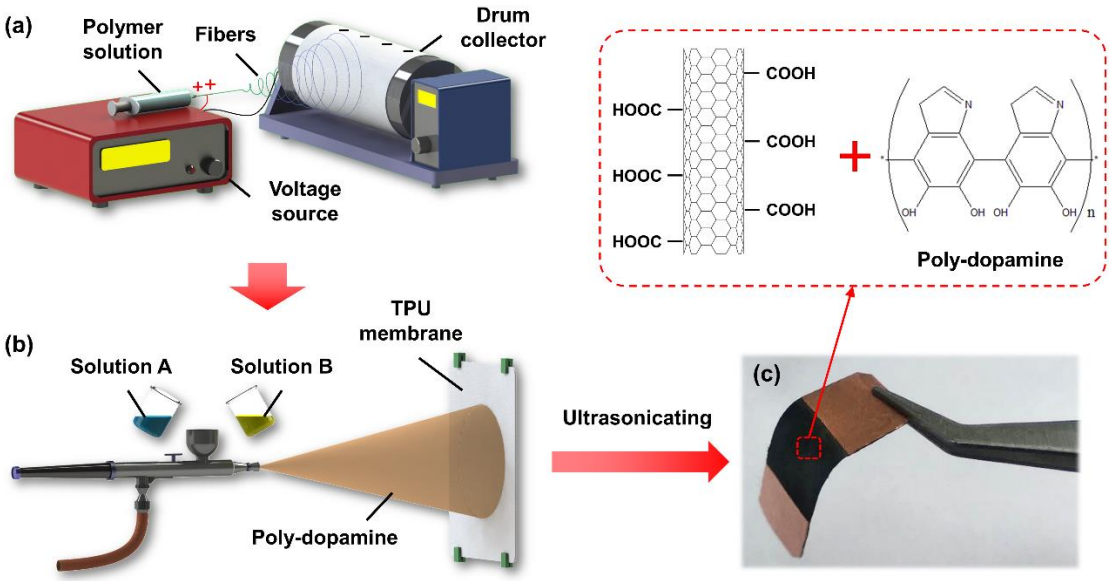

Figure 1 Schematic diagram of preparing conductive fibrous membrane: illustration of (a) fabricating TPU nanofibers and (b) DA modifying TPU nanofibers; (c) photo of DATPU/CNTs fibrous membrane.

Dopamine modification of electrospun TPU fibrous membrane

For the surface modification of electrospun TPU fibrous membrane, a 2.0 g/L aqueous solution of DA was prepared by dissolving the DA·HCl powder in distilled water and the pH of the solution was adjusted to 8.5 by adding Tris (the DA solution was termed as solution A). $NaIO_4$ aqueous solution with a concentration of 30 mM was noted as solution B. Solution A and solution B was mixed immediately and sprayed onto the TPU fibrous membrane. With the spontaneous deposition of an adherent poly-

dopamine (PDA) layer, the color of the mixture quickly changed from light pink to dark brown (Figure 1(b)). After 2 h, the TPU fibrous membrane was washed using distilled water and dried at 60 °C in a vacuum. The resultant TPU fibrous membranes were termed as DATPU.

Preparation of carboxyl CNTs

CNTs were treated by ultrasonicating in H_2SO_4/HNO_3 (3:1) mixed acid with a concentration of 10 g/L for 12 h, then stirring for 8 h at 65 °C. The mixture of carboxyl CNTs was centrifuged at 6000 r/min for 20 min and filtered through 0.22 μm filter paper. The modified CNTs were then washed to neutral with distilled water and dried in a vacuum at 40 °C. Detailed description of CNTs and carboxyl CNTs characterization was presented in the previous work [3]. Carboxyl CNTs were employed in the following work, which is also called CNTs in convenience.

Preparation of CNTs coated TPU fibrous membrane

Firstly, CNTs was added into distilled water to prepare the CNTs suspension with the concentration of 0.2 g/L, 0.4 g/L, 0.6 g/L, 0.8 g/L and 1.0 g/L. Both pure TPU and DATPU fibrous membranes with the size of 40 mm×10 mm were soaked into the above CNTs suspension. After ultrasonication for 60 min, the CNTs coated pure TPU and DATPU fibrous membrane were removed from the beaker, washed with distilled water for three times and placed in a vacuum oven at 60 °C for 24 h. The CNTs coated pure TPU and DATPU fibrous membranes were termed as TPU/CNTs-X and DATPU/CNTs-X, respectively (X means the concentration of CNTs suspension).

Characterization

The morphology of the samples was observed by using a scanning electron microscope (SEM) (Hitachi Regulus 8100, Tokyo, Japan).

Electrical sheet resistance of TPU/CNTs and DATPU/CNTs conductive fibrous

membrane was measured by using a multifunction digital four-probe tester (ST-2258C, Jiangsu, China).

Tensile tests were carried out by using a tensile testing machine (Instron-5965 Tensile Machine, Glenview, US) with the stretch rate of 100 mm/min. Rectangular specimens with the size of 40 mm×10 mm were used, and the clamping distance was 20 mm.

The surface chemical structure of the sample was carried out using X-ray photoelectron spectroscopy (XPS) (Thermo ESCALAB 250XI system Thermo Electron Corporation, USA) with an Al Kα X-ray source.

Thermogravimetric analysis (TGA) was performed using a DSC/TG synchronous thermal analyzer (STA449 F3 Jupiter, Bavaria, Germany) under nitrogen atmosphere. The sample, with a weight of 5-10 mg, was heated from room temperature to 800 °C with a heating rate of 20 °C/min.

The resistance of TPU/CNTs and DATPU/CNTs conductive fibrous membrane was measured with a digital multimeter (KEYSIGHT B2901A, US) which was equipped with a stepper motor to induce various tensile deformations in the tested samples.

Results and discussion

In this work, concentration of the CNTs suspension is a key factor in fabricating a conductive fibrous membrane with excellent conductivity. Therefore, CNTs suspension concentration was varied from 0.2 g/L, 0.4 g/L, 0.6 g/L, 0.8 g/L to 1.0 g/L to investigate its effect on the morphology, thermal properties and mechanical properties of conductive fibrous membrane. The morphology of resultant conductive fibrous membranes is depicted in Figure 2. As shown in Figure 2(a-f), the TPU fibers exhibited relatively smooth surface before ultrasonicating. As the concentration of CNTs suspension increased, there were more CNTs coated on the TPU fibers. However, by comparison with the pure TPU fibers, DATPU fibers possessed rougher surface, which

should be ascribed to the self-polymerization of DA on the surface of the TPU fiber, forming a poly-dopamine layer. Besides, DATPU fibrous membranes appeared to bind with more CNTs than TPU fibrous membrane for the same concentration of CNTs suspension.

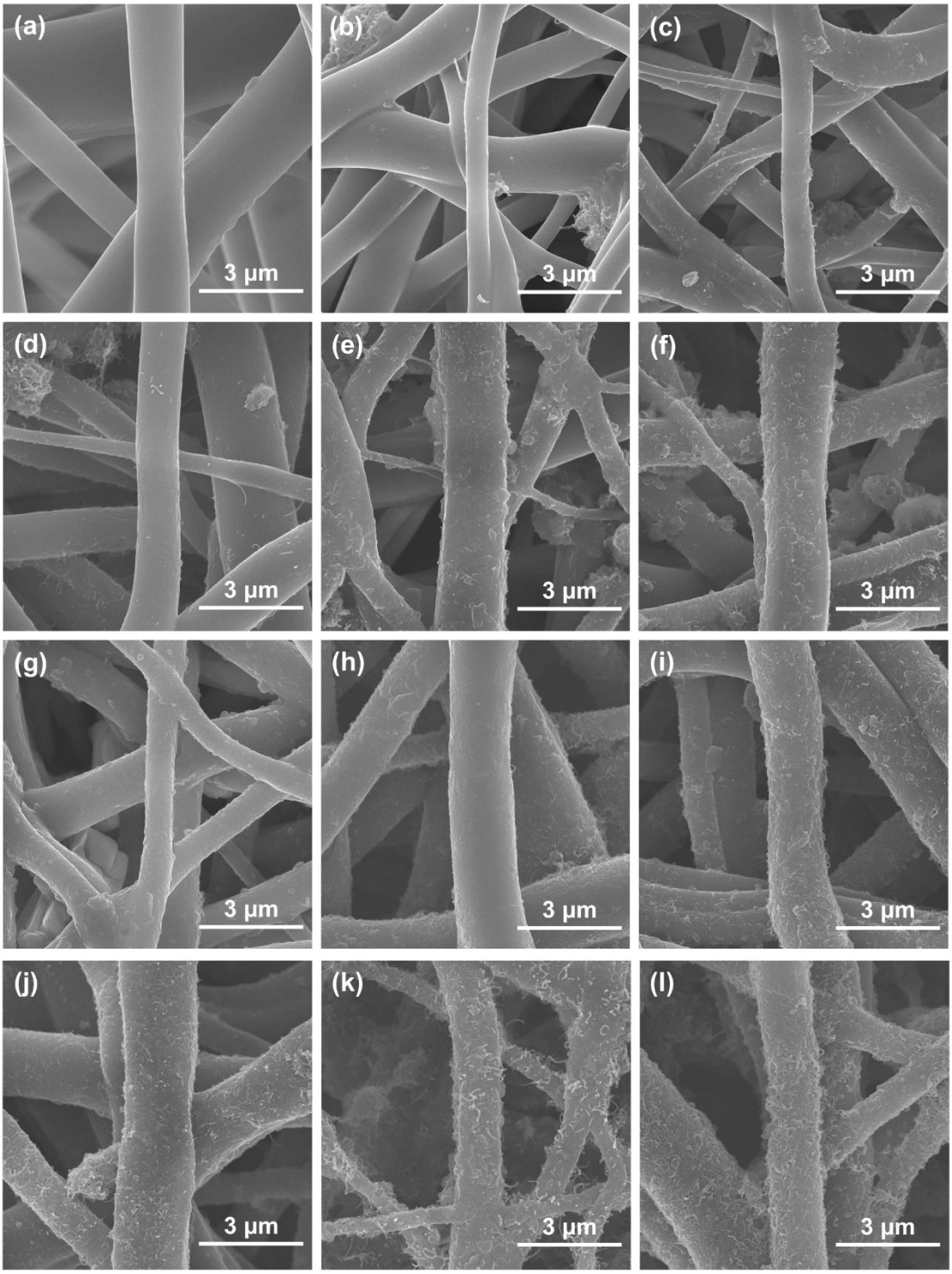

Figure 2 Morphology of (a) pure TPU; (b) TPU/CNTs-0.2; (c) TPU/CNTs-0.4; (d) TPU/CNTs-0.6; (e) TPU/CNTs-0.8; (f) TPU/CNTs-1.0; (g) DATPU; (h) DATPU/CNTs-0.2; (i) DATPU/CNTs-0.4; (j) DATPU/CNTs-0.6; (k) DATPU/CNTs-0.8; (l) DATPU/CNTs-1.0.

TGA was performed to determine the amount of CNTs coated on the fibrous membrane. As is shown in the Figure 3(a) and (c), when the temperature reached 800 °C, mass residue of pure TPU was about 8.93%, and the mass residues of TPU/CNTs-0.2, TPU/CNTs-0.4, TPU/CNTs-0.6, TPU/CNTs-0.8 and TPU/CNTs-1.0 were about 10.36%, 12.08%, 12.90%, 14.53% and 16.43%, which indicated that the content of CNTs coated on the TPU fibrous membranes were 1.57% (TPU/CNTs-0.2), 3.46% (TPU/CNTs-0.4), 4.36% (TPU/CNTs-0.6), 6.15% (TPU/CNTs-0.8) and 8.24% (TPU/CNTs-1.0), respectively. In contrast, for the TPU fibrous membranes modified with DA, the amount of CNTs on the DATPU fibrous membranes were about 3.31%, 5.67%, 7.13%, 8.76% and 9.79%, correspondingly. As is shown in Figure 3(b) and (d), the sheet resistance of the conductive membranes was inversely proportional to the content of CNTs coated. The sheet resistance of TPU/CNTs membranes decreased from 151.66±45.44 kΩ/sq to 0.65±0.14 kΩ/sq when the concentration of CNTs suspension increased from 0.2 g/L to 1.0 g/L. After being modified by DA, DATPU/CNTs offered a decrease of sheet resistance from 14.38±2.56 kΩ/sq to 0.32±0.11 kΩ/sq when the concentration of CNTs suspension increased from 0.2 g/L to 1.0 g/L. Notably, DATPU/CNTs exhibited lower sheet resistance than TPU/CNTs for the same concentration of CNTs suspension used. The results of the morphology proved that DATPU had a better ability to bind with CNTs, and the resultant conductive membranes possessed higher electrical conductivity. The relative higher amount of CNTs on

DATPU than TPU fibres should be responsible for the increase in electrical conductivity of DATPU/CNTs composites.

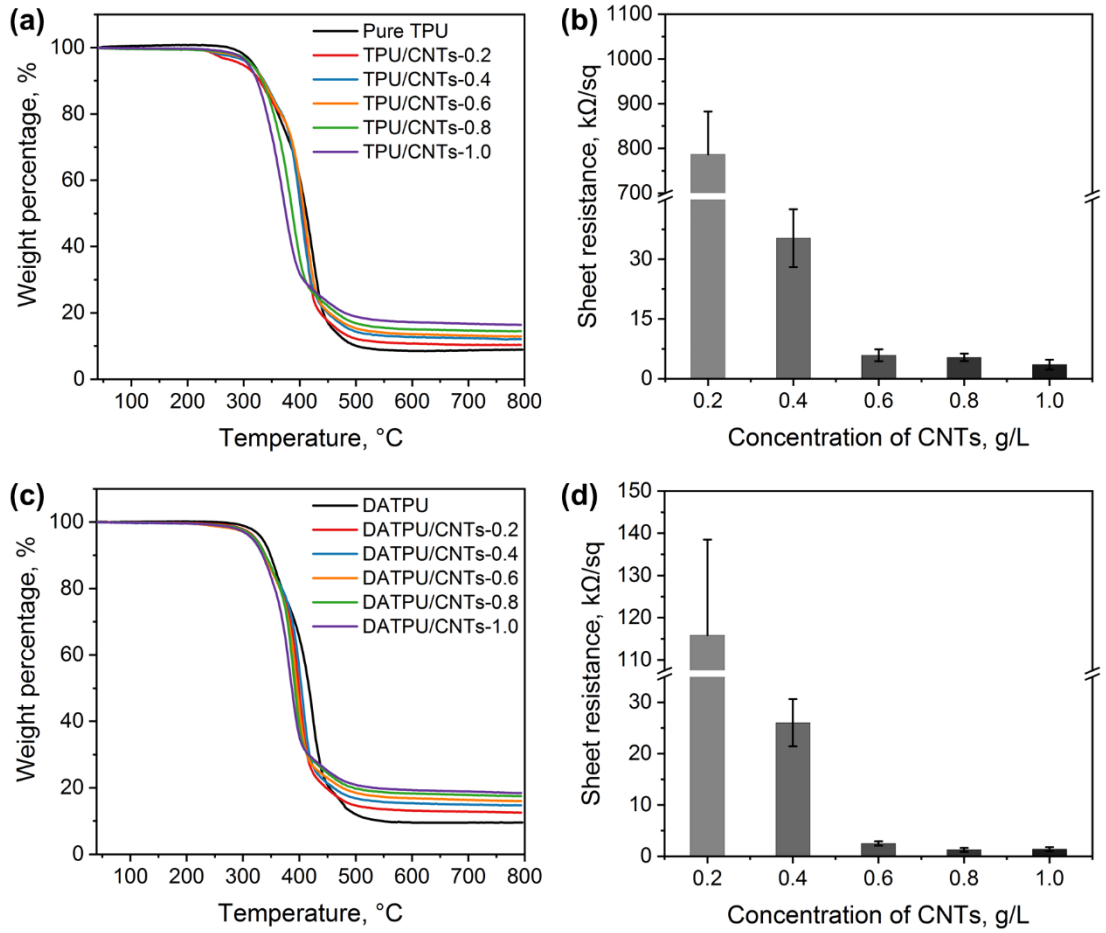

Figure 3 (a) TGA curves of pure TPU and TPU/CNTs fabricated using different CNTs suspension; (b) Histogram of sheet resistance of the TPU/CNTs fabricated using CNTs suspension with different concentration; (c) TGA curves of DATPU and DATPU/CNTs fabricated using CNTs suspension with different concentration; (d) Histogram of sheet resistance of the DATPU/CNTs fabricated using CNTs suspension with different concentration.

XPS spectra are demonstrated in Figure 4. As seen from the wide scan spectra of pure TPU and DATPU (Figure 4(a) and (b)), the peaks of C 1s, O 1s and N 1s were at 284.8 eV, 530.9 eV and 400.5 eV, respectively. From the C 1s core level spectrum of TPU shown in the Figure 4(c), one peak at 284.8 eV referred to the C-H/C-C groups, one

peak at 286.5 eV was related to C-O groups and another peak at 288.9 eV was attributed to NH-COO groups [33]. After coated with CNTs, there was a peak emerging at 283.6 eV referred to CNTs together with the other three peaks of C-H/C-C, C-O and NH-COO curve-fitting the C 1s core level spectrum of TPU/CNTs, as shown in Figure 4(d). As can been observed from Figure 4(e), a new peak of C-N at 285.3 eV in C 1s core level spectrum of DATPU appeared in comparison with pure TPU, indicating that the TPU fibrous membrane was modified by dopamine successfully [34]. The C 1s core level spectrum of DATPU/CNTs is exhibited in Figure 4(f), from which it can be seen that the peak of CNTs shifted to higher binding energy of 284.2 eV compared to that of TPU/CNTs. This is mainly due to the strong hydrogen bond between hydroxyl group and amino group on dopamine and the carboxyl group on the CNTs, resulting in that the carboxyl group becomes more electropositive [35]. Furthermore, because the dopamine and the -COOH group existed as cations and anions, respectively, it led to strong interactions between the CNTs and DATPU fibrous membrane [36]. In summary, the experimental results mentioned above confirmed that DA layer could bond the TPU fibers with CNTs tightly, resulting in an improved quantity of the CNTs coated on the DATPU and thus the conductivity of DATPU/CNTs remarkably.

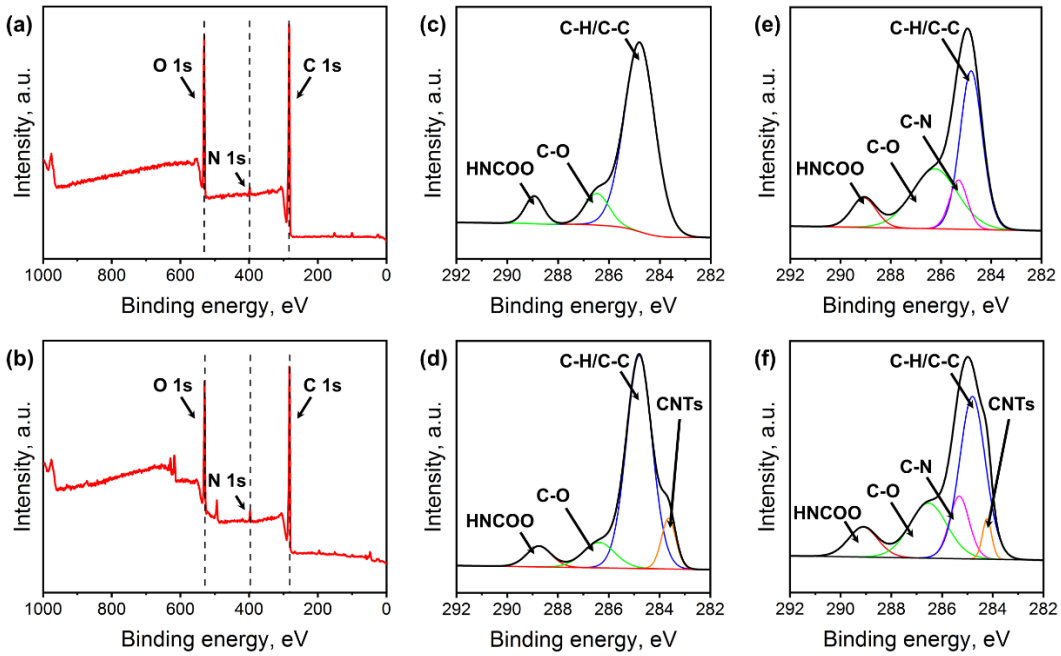

Figure 4 XPS wide scan spectra of (a) pure TPU and (b) DATPU; C 1s core level spectrum of (c) pure TPU; (d) TPU/CNTs; (e) DATPU; (f) DATPU/CNTs.

Mechanical properties are the crucial indicators for evaluating materials in practical applications. The typical stress-strain curves of conductive composite fibrous membranes are shown in Figure 5. It can be seen from the Figure 5 and Table 1 that the tensile strength of the conductive fibrous membrane increased with increasing concentration of CNTs suspension for both TPU and DATPU nanofibers. For example, the TPU/CNTs-1.0 possessed a tensile strength of 11.15±0.12 MPa, which was about 2.80 MPa higher than pure TPU, while the tensile strength of DATPU/CNTs-1.0 was 11.75±0.15 MPa, which was about 3.19 MPa higher than DATPU. This obviously enhanced tensile strength might benefit from the significant reinforce effect of CNTs [37]. In addition, as mentioned previously in this study, DA coating layer, which has a strong interaction with TPU fibers, could led to a higher tensile strength of DATPU (8.56±0.33 MPa) than that of pure TPU (8.35±0.21 MPa) [38]. Owing to the amount of CNTs coated on DATPU was higher than that of TPU, DATPU/CNTs fibrous membranes exhibited higher tensile strength than TPU/CNTs. However, the elongation

at break slightly decreased from 1043±39% to 934±30% after the TPU fibrous membranes were modified via DA, as shown in Figure 5b. This might be because that DA layer as well as the CNTs interconnected the fibers, facilitating a decreasing slippage of between fibers [11]. Due to the excellent electrical conductivity and mechanical property, the conductive DATPU/CNTs fibrous membrane- prepared using 1.0 g/L of CNTs suspension were chosen for further investigation on the electromechanical properties. For convenience of reading, TPU/CNTs-1.0 and DATPU/CNTs-1.0 are abbreviated as TPU/CNTs and DATPU/CNTs respectively in the following.

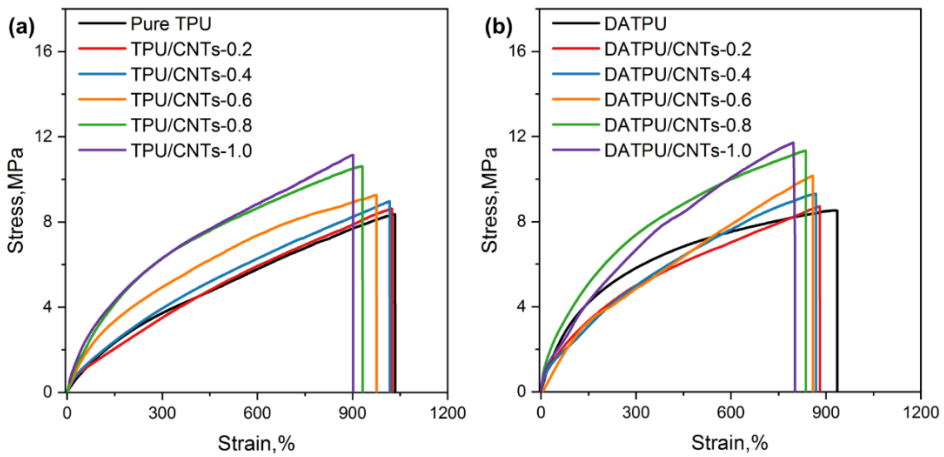

Figure 5 Strain-stress curves of (a) pure TPU and TPU/CNTs fabricated using different CNTs suspension; (b) DATPU and DATPU/CNTs fabricated using different CNTs suspension.

Table 1 Mechanical properties: tensile strength (σ) and elongation at break ($\varepsilon_{at\ break}$)

Sample	σ (MPa)	$\varepsilon_{at\ break}$ (%)	Sample	σ (MPa)	$\varepsilon_{at\ break}$ (%)
Pure TPU	8.35±0.21	1043±39	DATPU	8.56±0.33	934±30
TPU/CNTs-0.2	8.63±0.17	1025±18	DATPU/CNTs-0.2	8.75±0.11	889±25
TPU/CNTs-0.4	8.96±0.20	1014±16	DATPU/CNTs-0.4	9.37±0.16	866±34
TPU/CNTs-0.6	9.25±0.23	982±18	DATPU/CNTs-0.6	10.16±0.16	852±40
TPU/CNTs-0.8	10.62±0.19	934±33	DATPU/CNTs-0.8	11.38±0.35	832±27
TPU/CNTs-1.0	11.15±0.12	903±29	DATPU/CNTs-1.0	11.75±0.15	807±27

In this work, the electrical properties such as relative resistance ($\Delta R/R_0$, $\Delta R=R-R_0$, R is the real-time resistance, R_0 represents the original resistance) and gauge factor (GF) ($(\Delta R/R_0)/\varepsilon$, ε is the strain) were characterized. The gauge factor was defined as the ratio of the change of relative resistance to the change of strain. As shown in Figure 6(a) and (b), the TPU/CNTs membrane exhibited a wide working range of 560% with a high GF of 130. In contrast, DATPU/CNTs possessed a larger working range of 710% (as shown in Figure 6 (d)), which was 1.5 times larger than that of TPU/CNTs. For the sensitivity, the DATPU/CNTs exhibited a GF as high as 1200, which was 9 times higher than that of TPU/CNTs (Figure 6(e)). The *I-V* curves of the TPU/CNTs and DATPU/CNTs acquired under the strain of 0%, 50%, 100%, 200%, 400% and 600%, are shown in Figure 6(c) and (f). The *I-V* curves for TPU/CNTs membranes and DATPU/CNTs membranes in the strain range from 0% to 400% were linear, indicating an excellent conductivity. When the strain exceeded 600%, the nonlinear *I-V* curve of TPU/CNTs indicated poor conductivity, while the linear *I-V* curve of DATPU/CNTs proved good conductivity.

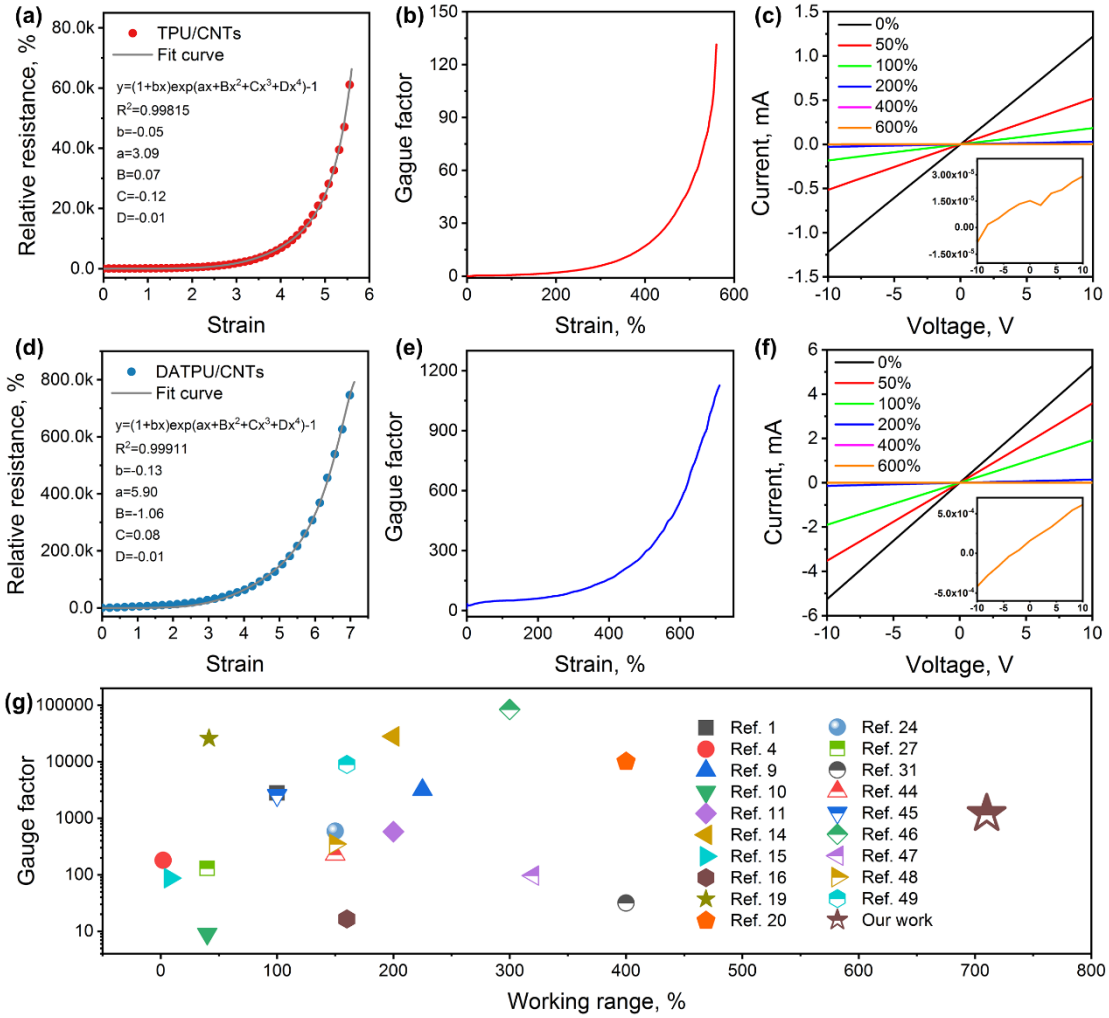

Figure 6 (a) The relative resistance-strain fitting curve of TPU/CNTs; (b) The guage factor (GF) versus strain curve of TPU/CNTs; (c) I-V curves under different applied strain of TPU/CNTs; (d) The relative resistance-strain fitting curve of DATPU/CNTs; (e) The gauge factor (GF) versus strain curve of DATPU/CNTs; (f) I-V curves under different applied strain of DATPU/CNTs; (g) comparison of the GF and the maximum working range reported between the references and our work.

As shown in Figure 6(a) and (d), the experimental data of relative resistance related to strain was fitted theoretically according to the "tunnel effect" [39, 40], whose model reported that the total electrical resistance *R* of the conductive polymer can be determined by Equation (1) and (2) below [41, 42].

$$R = \left(\frac{L}{N}\right)\left(\frac{8\pi hs}{3\gamma a^2 e^2}\right)\exp(\gamma s) \quad (1)$$

$$\gamma = \frac{4\pi\sqrt{2m\varphi}}{h} \quad (2)$$

where N refers to the number of conductive paths, L is related to the number of particles forming a conductive path, h is the Plank constant, s represents the smallest distance between the CNTs, a^2 represents the effective cross section and e is about the electron change, respectively. Besides, in the Equation (2), m is the electron mass and φ is related to the height of potential barrier between adjacent CNTs.

As the strain is applied to the conductive fibrous membranes, the resistance would increase owing to the damage of CNTs conductive networks. It can be assumed that the distance between CNTs varies from s_0 (original distance between CNTs) to s under the external force and the quantity of conductive paths decreased from N_0 (the quantity of conductive paths in the original state) to N, s and N can be calculated according Equation (3) and (4) [43].

$$s = s_0(1+b\varepsilon) \quad (3)$$

$$N = \frac{N_0}{\exp\left(A\varepsilon + B\varepsilon^2 + C\varepsilon^3 + D\varepsilon^4\right)} \quad (4)$$

where b, A, B, C, D are constant. Substituting Equation (3) and (4) into Equation (1), it can be obtained that:

$$\frac{\Delta R}{R_0} = \frac{R - R_0}{R_0} = \left(\frac{sN_0}{Ns_0}\right)\exp\left[\gamma\left(s - s_0\right)\right] - 1 = \left(1+b\varepsilon\right)\exp\left[\left(A + \gamma b s_0\right)\varepsilon + B\varepsilon^2 + C\varepsilon^3 + D\varepsilon^4\right] - 1 \quad (5)$$

As presented in Figure 6(a) and (d), the experimental data of both TPU/CNTs and DATPU/CNTs are in good agreement with the theoretical values calculated from Equations (5) with R^2 value of 0.99815 and 0.99911, respectively. As shown in the Figure 6(g), compared with the strain sensors reported in previous work [1, 4, 9-11, 14-

16, 19, 20, 24, 27, 31, 44-49], the integration of ultra-high working range and high GF leads DATPU/CNTs strain sensor to stand out, indicating a feasibility of its application in monitoring large strains.

In order to determine the fastness of CNTs coated on the fibrous membranes, DATPU/CNTs were immersed in distilled water and ultrasonicated for 20 min, 40 min, 60 min and 80 min. The morphology, TG analysis and sheet resistance of the samples after washing are shown in Figure 7. It can be seen from the SEM image that after washing for 80 min, the quantity of CNTs coating on TPU decreased considerably (Figure 7(a)), which could be caused by the removal of some CNTs during ultrasonication. In contrast, there were still a large amount of CNTs adhering to the DATPU fibrous membrane after washing for 80 min, which should be due to the strong binding between CNTs and DATPU fibers. The weight loss determined from TG analysis of TPU/CNTs after washing for 20 min, 40 min, 60 min and 80 min (as shown in Figure 7 (c)) was 86.58%, 87.62%, 88.86% and 89.47%, corresponding to the loss content of CNTs after washing of 3.31%, 4.45%, 5.81% and 6.48%, respectively. In the case of the DATPU/CNTs, the content of CNTs washed away after ultrasonicating for 20 min, 40 min, 60 min and 80 min was 1.66%, 2.47%, 3.31% and 4.04%, which were about 50% less than those TPU/CNTs samples washed the same time. Besides, the sheet resistance of TPU/CNTs increased from 5.36±0.95 kΩ/sq to 102.83±7.51kΩ/sq, while the sheet resistance of DATPU/CNTs only increased from 1.25±0.36 kΩ/sq to 15.67±3.66 kΩ/sq after washing for 80 min. These results revealed that the adhesion between DATPU fibrous membranes and CNTs was stronger than TPU fibrous membranes and CNTs.

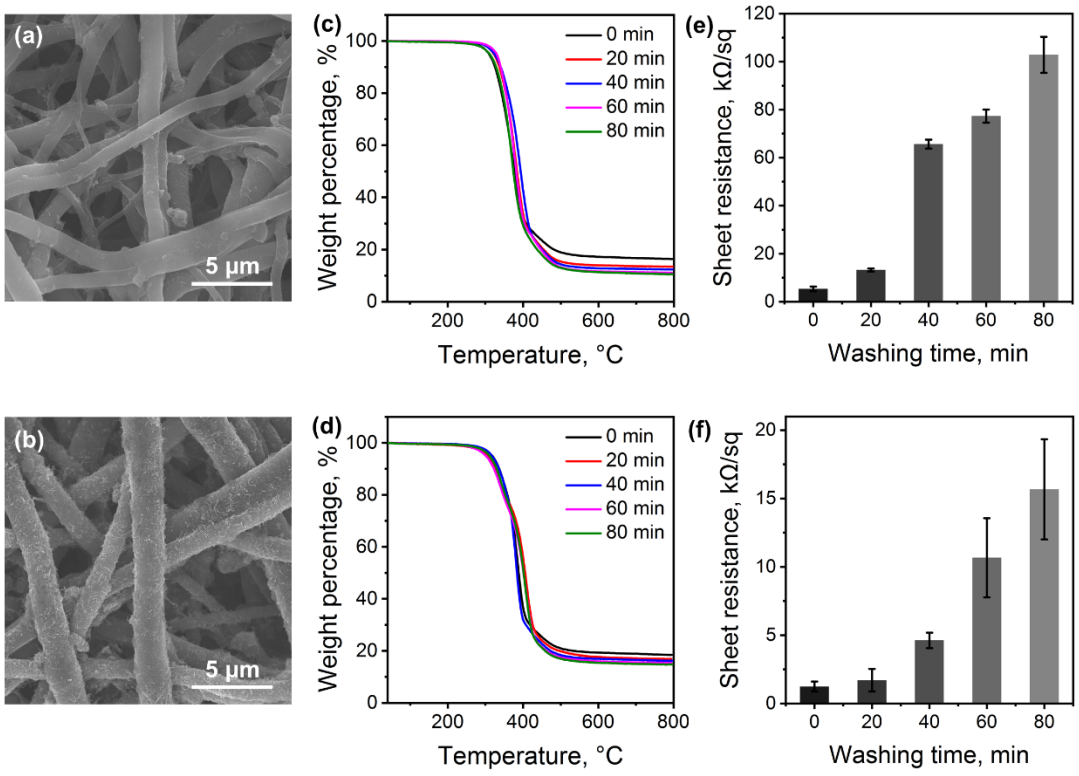

Figure 7 Morphology of (a) TPU/CNTs and (b) DATPU/CNTs after washing for 80 min; TGA curves of (c) TPU/CNTs and (d) DATPU/CNTs after washing for different time; Histogram of the sheet resistance of (e) TPU/CNTs and (f) DATPU/CNTs after washing for different time.

Figure 8 displays the sensing behavior of DATPU/CNTs at different strain ranging from 0 to 50%, 100%, 200%, 400% and 600%. It can be seen that the DATPU/CNTs conductive fibrous membrane exhibited the ability to maintain its electrical conductivity across all strain ranges. However, it should be noted that during the first four stretching-releasing cycles, the values of relative resistance did not reach a steady state, and then became constant gradually with the increasing stretching-releasing cycle number. The reason behind this can be explained from the following two aspects: the hysteresis and changes of conductive path [28] in the stretching-releasing process. As shown in Figure 8(b) and (c), when applying 50%, 100%, 200%, 400% and 600% strain of stretching-releasing to the DATPU/CNTs fibrous membranes, the mechanical

hysteresis, which was calculated according to the integration of stretching-releasing curve in each cycle, decreased obviously at the first cycle for all of the strain degrees, when the cycle number exceeded 3, the mechanical hysteresis kept stable basically. For example, under the stretching-releasing test in the strain range from 0 to 600%, the mechanical hysteresis at the first cycle was 31.87 MJ/m^3 and then decreased sharply to 4.85 MJ/m^3 at the 2^{nd} cycle and eventually remained at around 3.00 MJ/m^3 from the 3^{rd} cycle. This should be ascribed to the Mullins effect, the broken of some weak polymer chains led to a decreased number of polymer chains maintained stress. Besides, DATPU fibers macromolecular network and DATPU fibrous network rearranged, conducting to stress decreasing [50, 51].

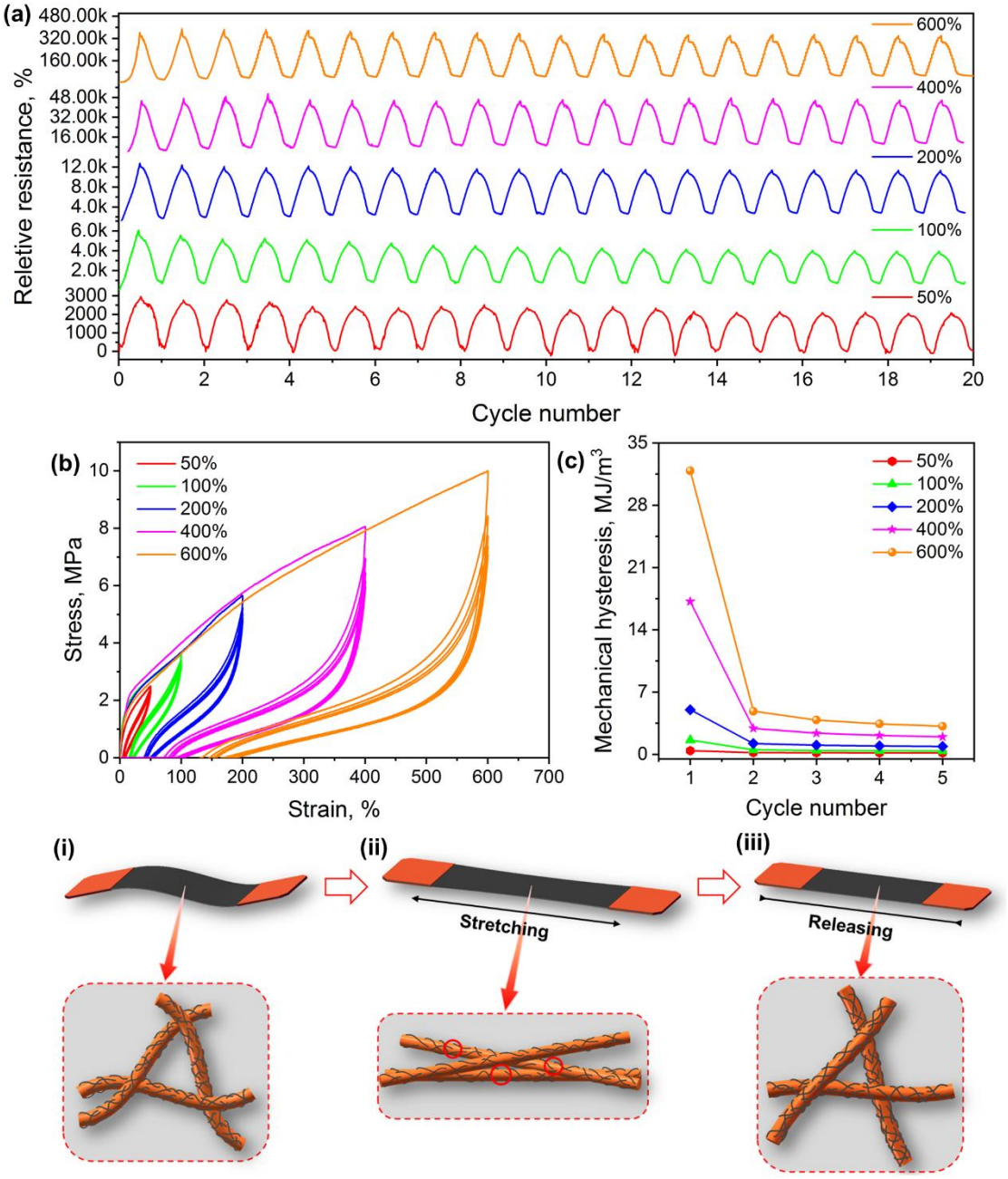

Figure 8 (a) curves of relative resistance related to 20 cycles of stretching-releasing test applied over different strain ranges: 0-50%, 0-100%, 0-200%, 0-400% and 0-600% with a constant stretching rate of 10 mm/min; (b) elastic recovery curves for five cycles stretching-releasing test of DATPU/CNTs with strain of 0-50%, 0-100%, 0-200%, 0-400% and 0-600%; (c) mechanical hysteresis of elastic recovery for DATPU/CNTs with strains of 50%-600%; schematic of the CNTs conductive network in the (i) original stage; (ii) stretching stage; (iii) releasing stage.

The schematic describing the change in CNTs conductive network in one cycle of stretching-releasing test is shown in Figure 8(i-iii). Figure 8(i) exhibits the original CNTs conductive network before stretching, which was relatively compact. Then, some of the conductive pathways were broken after stretching was applied to DATPU/CNTs (shown in Figure 8(ii)), leading to an increasing electrical resistance. However, when the stretching was released (shown in Figure 8(iii)), the conductive network could reconstruct. Therefore, the proposed break-connection of the conductive pathways upon stretching-releasing could result in relatively large variations in the value of relative resistance observed in the first few stretching-releasing tests, while once the conductive pathways were adapted to the applied stretching-releasing process, the variation in the value of relative resistance became constant with increasing the number of stretching-releasing cycles.

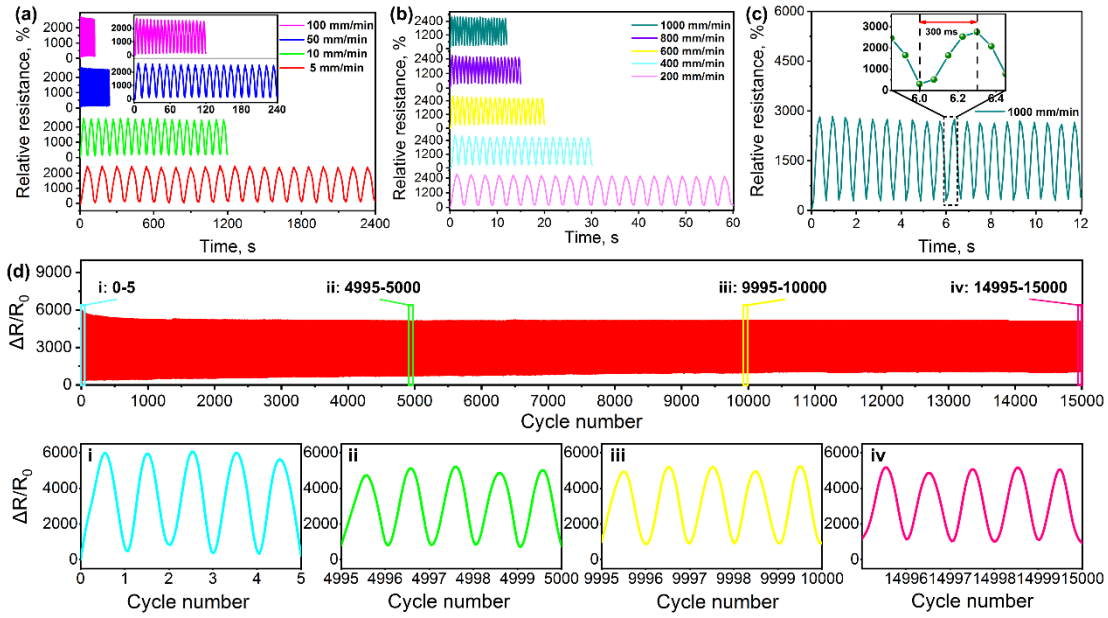

Figure 9 (a-b) curves of relative resistance under 50% strain at the stretch rate of 5 mm/min, 10 mm/min, 50 mm/min, 100 mm/min, 200 mm/min, 400 mm/min, 600 mm/min, 800 mm/min and 1000 mm/min for 20 cycles of stretching-releasing test; (c) response time for 50% abrupt strain; (d) working durability under 100% of strain for

15000 cycles of stretching-releasing test. (i-iv) show the sensing behavior in 0-5, 4995-5000, 9995-10000 and 14995-15000 cycles, respectively.

The sensing behavior of DATPU/CNTs under the stretching rates of 5 mm/min, 10 mm/min, 50 mm/min, 100 mm/min, 200 mm/min, 400 mm/min, 600 mm/min, 800 mm/min and 1000 mm/min was performed and illustrated in Figure 9(a) and (b). As can be seen from these two figures, no obvious changes in relative resistance were presented at each stretching rate, indicating that DATPU/CNTs had excellent ability to sense different external stimuli across all stretching rates. In particular, as can be seen from Figure 9(c), the strain sensor had a rapid response time of 300 ms to the abrupt strain sweep up to 50% by applying a stretch rate of 1000 mm/min. Moreover, as shown in Figure 9(d), 15000 cycles of stretching-releasing test were performed under 100% of strain and 100 mm/min of stretch rate, revealing a good durability of electrical resistance. For instance, the relative resistance was about 300% in the first 5 cycles, about 240% in 4995-5000 cycles, and remained about 240% in the following 9995-10000 and 14995-15000 cycles, revealing a good working stability of DATPU/CNTs based strain sensor.

The DATPU/CNTs composite conductive fibrous membrane was used for human motions detection in this work due to the advantages of high working range, good sensitivity, excellent stability and outstanding durability. DATPU/CNTs was fixed on the Adam's apple, fingers, wrist and knee of a volunteer, who had read and signed the consent form. As shown in Figure 10(a-d), from a tiny swallow movement (Figure 10(a)), a small finger bending movement (Figure 10(b)), through a middle wrist bending movement (Figure 10(c)) to a large knee bending movement (Figure 10(d)), the DATPU/CNTs showed high and repeatable sensitivity to these motions in the testing cycles. Besides, the response of DATPU/CNTs was found to vary the degree of

bending. For example, as the finger bending changed from 0° through 45° to 90°, the value of relative resistance changed by about 2000% and 3500%, respectively. Figure 10(i-iv) exhibits the gradual decrease in brightness of a light emitting diode (LED) with the increasing stretching up to 200% of the DATPU/CNTs membrane that was connected into an electric circuit (see Movie S1), revealing that the electrical resistance of DATPU/CNTs increased with increasing strain.

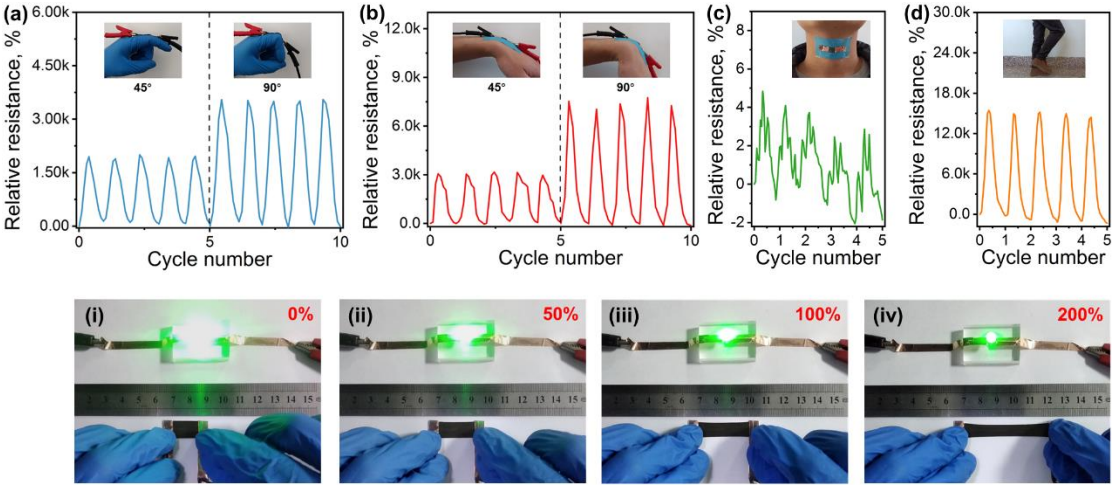

Figure 10 (a) Relative resistance obtain in real time from the human motion (a) figure bending; (b) wrist bending; (c) swallow; (d) knee bending; The brightness of LED changed with the DATPU/CNTs strain sensor stretched from (i) 0% to (ii) 50%; (iii) 100%; (iv) 200%.

A smart motion detection prototype kneecap was constructed by integrating the DATPU/CNTs strain sensor, Bluetooth device and battery. The diagram of the smart kneecap device and its main hardware components and photo are shown in Figure 11(a-b). The current signals generated from the volunteer's knee motions could be transmitted to the smart phone in real time by the Bluetooth device in the smart kneecap. The practical working condition of the smart motion detection kneecap is shown in Figure 11(c-h) and the supplementary Movie S2. At the original stage (Figure 11 (c)), a constant current signal (80 mA) was detected on the right knee of the standing-straight

volunteer, while a regularly variable current signal (about -20 mA) was seen on the right knee with a fixed bending of about 100° (Figure 11(d)). As shown in Figure 11(e and f), when the volunteer was walking (40 steps/min) and running (80 steps/min), the frequency of current signal changed corresponding to the changes in the variable knee bending frequency. In addition, as shown in Figure 11(g), the smart motion detection kneecap had a good response to human squatting movement (100° bending angle for -20 mA current change). Finally, when the human movement stopped (ending stage shown in Figure (h)), the current signal value (77 mA) returned to the same current value to the initial stage, which further confirmed the stability of the smart motion detection kneepad. These results indicated that the developed smart motion detection kneecap can sensitively and repeatedly respond to the different movements of human body.

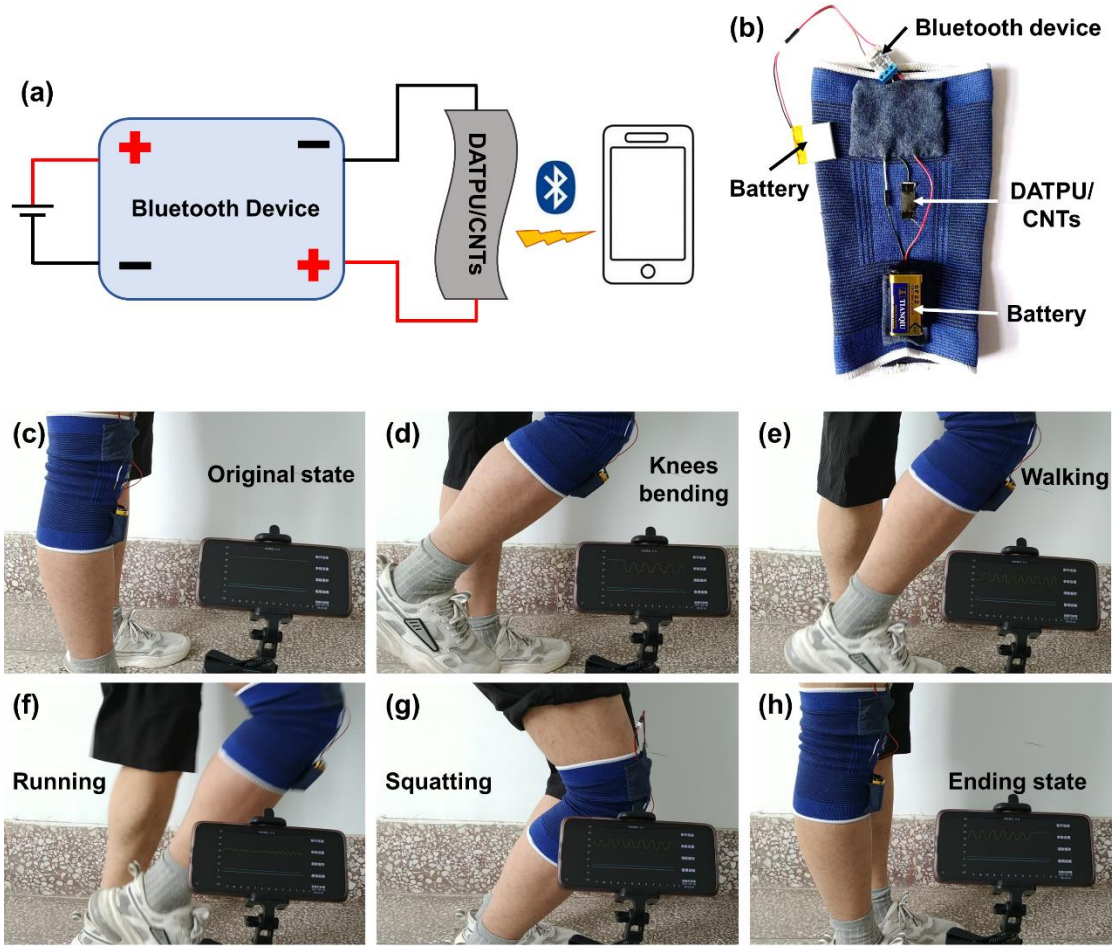

Figure 11 (a) diagram of main hardware circuit of the smart motion detection kneecap; (b) smart motion detection kneecap; detecting the human motion of (c) original state; (d) knees bending; (e) walking; (f) running; (g) squatting; (h) ending state using smart motion detection kneecap.

Conclusion

In this work, a strain sensor with ultra-high working range was fabricated by coating CNTs on the TPU electrospun fibrous membrane via ultrasonication. The amount and fastness of CNTs coated on the TPU fibrous membrane was enhanced by utilizing the rapid dopamine modification assisted with $NaIO_4$. As demonstrated in the results, DATPU/CNTs exhibited ultra-high working range of 710% with a good sensitivity of GF up to 1200. Due to the dopamine layer, DATPU/CNTs represented an excellent washing fastness. In addition, under different stretching rate and strain level, the DATPU/CNTs membrane displayed a good working stability. An excellent durability and a good reproducibility were observed during 15000 cycles of stretching-releasing test. Finally, DATPU/CNTs can accurately sense different degrees of human movement, such as finger bending, swallow, wrist bending and knee bending, indicating great promising for application in wearable devices.

Acknowledgment

The authors gratefully acknowledge the National Natural Science Foundation of China (Grant no. 51703108 and Grant no. 52003130), the Postdoctoral Science Foundation of China (Grant no. 2019M652318) and Taishan Scholar Foundation of Shandong, China (Grant no. tsqn201909100) for financial support.

References

[1] Z. He, G. Zhou, J.-H. Byun, S.-K. Lee, M.-K. Um, B. Park, T. Kim, S.B. Lee, T.-W.

Chou, Highly stretchable multi-walled carbon nanotube/thermoplastic polyurethane composite fibers for ultrasensitive, wearable strain sensors, Nanoscale, 11 (2019) 5884-5890.

[2] G. Zhou, J.-H. Byun, Y. Oh, B.-M. Jung, H.-J. Cha, D.-G. Seong, M.-K. Um, S. Hyun, T.-W. Chou, Highly sensitive wearable textile-based humidity sensor made of high-strength, single-walled carbon nanotube/poly (vinyl alcohol) filaments, ACS applied materials & interfaces, 9 (2017) 4788-4797.

[3] B. Zhou, Z. Liu, C. Li, M. Liu, L. Jiang, Y. Zhou, F.L. Zhou, S. Chen, S. Jerrams, J. Yu, A Highly Stretchable and Sensitive Strain Sensor Based on Dopamine Modified Electrospun SEBS Fibers and MWCNTs with Carboxylation, Advanced Electronic Materials, (2021) 2100233.

[4] Y. Ma, N. Liu, L. Li, X. Hu, Z. Zou, J. Wang, S. Luo, Y. Gao, A highly flexible and sensitive piezoresistive sensor based on MXene with greatly changed interlayer distances, Nature communications, 8 (2017) 1-8.

[5] J. Di, X. Zhang, Z. Yong, Y. Zhang, D. Li, R. Li, Q. Li, Carbon‐nanotube fibers for wearable devices and smart textiles, Advanced materials, 28 (2016) 10529-10538.

[6] C. Yan, J. Wang, W. Kang, M. Cui, X. Wang, C.Y. Foo, K.J. Chee, P.S. Lee, Highly stretchable piezoresistive graphene–nanocellulose nanopaper for strain sensors, Advanced materials, 26 (2014) 2022-2027.

[7] L. Jiang, Y. Wang, X. Wang, F. Ning, S. Wen, Y. Zhou, S. Chen, A. Betts, S. Jerrams, F.-L. Zhou, Electrohydrodynamic printing of a dielectric elastomer actuator and its application in tunable lenses, Composites Part A: Applied Science and Manufacturing,

147 (2021) 106461.

[8] S. Seyedin, P. Zhang, M. Naebe, S. Qin, J. Chen, X. Wang, J.M. Razal, Textile strain sensors: a review of the fabrication technologies, performance evaluation and applications, Materials Horizons, 6 (2019) 219-249.

[9] Y. Zhao, M. Ren, Y. Shang, J. Li, S. Wang, W. Zhai, G. Zheng, K. Dai, C. Liu, C. Shen, Ultra-sensitive and durable strain sensor with sandwich structure and excellent anti-interference ability for wearable electronic skins, Composites Science and Technology, 200 (2020) 108448.

[10] X. Fu, M. Ramos, A.M. Al-Jumaily, A. Meshkinzar, X. Huang, Stretchable strain sensor facilely fabricated based on multi-wall carbon nanotube composites with excellent performance, Journal of Materials Science, 54 (2019) 2170-2180.

[11] Y. Li, B. Zhou, G. Zheng, X. Liu, T. Li, C. Yan, C. Cheng, K. Dai, C. Liu, C. Shen, Continuously prepared highly conductive and stretchable SWNT/MWNT synergistically composited electrospun thermoplastic polyurethane yarns for wearable sensing, Journal of Materials Chemistry C, 6 (2018) 2258-2269.

[12] T. Yan, Z. Wang, Z.-J. Pan, Flexible strain sensors fabricated using carbon-based nanomaterials: A review, Current Opinion in Solid State and Materials Science, 22 (2018) 213-228.

[13] S. Gong, D.T. Lai, B. Su, K.J. Si, Z. Ma, L.W. Yap, P. Guo, W. Cheng, Highly stretchy black gold E‐Skin nanopatches as highly sensitive wearable biomedical sensors, Advanced Electronic Materials, 1 (2015) 1400063.

[14] X. Yue, Y. Jia, X. Wang, K. Zhou, W. Zhai, G. Zheng, K. Dai, L. Mi, C. Liu, C.

Shen, Highly stretchable and durable fiber-shaped strain sensor with porous core-sheath structure for human motion monitoring, Composites Science and Technology, 189 (2020) 108038.

[15] T. Huang, P. He, R. Wang, S. Yang, J. Sun, X. Xie, G. Ding, Porous fibers composed of polymer nanoball decorated graphene for wearable and highly sensitive strain sensors, Advanced Functional Materials, 29 (2019) 1903732.

[16] L. Tong, X.X. Wang, X.X. He, G.D. Nie, J. Zhang, B. Zhang, W.Z. Guo, Y.Z. Long, Electrically Conductive TPU Nanofibrous Composite with High Stretchability for Flexible Strain Sensor, Nanoscale Research Letters, 13 (2018) 86.

[17] Y. Wang, W. Li, Y. Zhou, L. Jiang, J. Ma, S. Chen, S. Jerrams, F. Zhou, Fabrication of high-performance wearable strain sensors by using CNTs-coated electrospun polyurethane nanofibers, Journal of Materials Science, 55 (2020) 12592-12606.

[18] M. Amjadi, Y.J. Yoon, I. Park, Ultra-stretchable and skin-mountable strain sensors using carbon nanotubes–Ecoflex nanocomposites, Nanotechnology, 26 (2015) 375501.

[19] W. Li, Y. Zhou, Y. Wang, L. Jiang, J. Ma, S. Chen, F.L. Zhou, Core–Sheath Fiber‐Based Wearable Strain Sensor with High Stretchability and Sensitivity for Detecting Human Motion, Advanced Electronic Materials, 7 (2021) 2000865.

[20] W. Li, Y. Zhou, Y. Wang, Y. Li, L. Jiang, J. Ma, S. Chen, Highly Stretchable and Sensitive SBS/Graphene Composite Fiber for Strain Sensors, Macromolecular Materials and Engineering, 305 (2020) 1900736.

[21] J.R. Bautista-Quijano, P. Pötschke, H. Brünig, G. Heinrich, Strain sensing, electrical and mechanical properties of polycarbonate/multiwall carbon nanotube

monofilament fibers fabricated by melt spinning, Polymer, 82 (2016) 181-189.

[22] M. Cai, H. He, X. Zhang, X. Yan, J. Li, F. Chen, D. Yuan, X. Ning, Efficient Synthesis of PVDF/PI Side-by-Side Bicomponent Nanofiber Membrane with Enhanced Mechanical Strength and Good Thermal Stability, Nanomaterials, 9 (2018) 39.

[23] Y. Liu, H. Zheng, M. Liu, High performance strain sensors based on chitosan/carbon black composite sponges, Materials & Design, 141 (2017) 276-285.

[24] G. Li, K. Dai, M. Ren, Y. Wang, G. Zheng, C. Liu, C. Shen, Aligned flexible conductive fibrous networks for highly sensitive, ultrastretchable and wearable strain sensors, Journal of Materials Chemistry C, 6 (2018) 6575-6583.

[25] P. Costa, M.F. Carvalho, V. Correia, J.C. Viana, S. Lanceros-Méndez, Polymer Nanocomposite-Based Strain Sensors with Tailored Processability and Improved Device Integration, ACS Applied Nano Materials, 1 (2018) 3015-3025.

[26] L. Lu, X. Wei, Z. Ye, G. Zheng, K. Dai, C. Liu, C. Shen, A flexible and self-formed sandwich structure strain sensor based on AgNW decorated electrospun fibrous mats with excellent sensing capability and good oxidation inhibition properties, Journal of Materials Chemistry C, 5 (2017) 7035-7042.

[27] H. Gong, C. Cai, H. Gu, Q. Jiang, D. Zhang, Z. Cheng, Flexible and wearable strain sensor based on electrospun carbon sponge/polydimethylsiloxane composite for human motion detection, RSC Advances, 11 (2021) 4186-4193.

[28] M. Ren, Y. Zhou, Y. Wang, G. Zheng, K. Dai, C. Liu, C. Shen, Highly stretchable and durable strain sensor based on carbon nanotubes decorated thermoplastic polyurethane fibrous network with aligned wave-like structure, Chemical Engineering

Journal, 360 (2019) 762-777.

[29] R. Wang, N. Jiang, J. Su, Q. Yin, Y. Zhang, Z. Liu, H. Lin, F.A. Moura, N. Yuan, S. Roth, A Bi‐Sheath Fiber Sensor for Giant Tensile and Torsional Displacements, Advanced Functional Materials, 27 (2017) 1702134.

[30] W. Zeng, L. Shu, Q. Li, S. Chen, F. Wang, X.M. Tao, Fiber‐based wearable electronics: a review of materials, fabrication, devices, and applications, Advanced materials, 26 (2014) 5310-5336.

[31] M. Xu, J. Qi, F. Li, Y. Zhang, Highly stretchable strain sensors with reduced graphene oxide sensing liquids for wearable electronics, Nanoscale, 10 (2018) 5264-5271.

[32] Z. Cui, J. Lin, C. Zhan, J. Wu, S. Shen, J. Si, Q. Wang, Biomimetic composite scaffolds based on surface modification of polydopamine on ultrasonication induced cellulose nanofibrils (CNF) adsorbing onto electrospun thermoplastic polyurethane (TPU) nanofibers, Journal of Biomaterials Science, Polymer Edition, 31 (2020) 561-577.

[33] P. Alves, S. Pinto, H.C. de Sousa, M.H. Gil, Surface modification of a thermoplastic polyurethane by low‐pressure plasma treatment to improve hydrophilicity, Journal of Applied Polymer Science, 122 (2011) 2302-2308.

[34] L. Shanmugam, X. Feng, J. Yang, Enhanced interphase between thermoplastic matrix and UHMWPE fiber sized with CNT-modified polydopamine coating, Composites Science and Technology, 174 (2019) 212-220.

[35] S. Liu, C.-M. Chan, L.-T. Weng, L. Li, M. Jiang, Surface Characterization of Poly

(styrene-co-p-hexafluoro-hydroxyisopropyl-α-methylstyrene)/Poly (4-vinylpyridine) Blends Spanning the Immiscibility− Miscibility− Complexation Transition by XPS, ToF-SIMS, and AFM, Macromolecules, 35 (2002) 5623-5629.

[36] H. Bi, Y. Li, S. Liu, P. Guo, Z. Wei, C. Lv, J. Zhang, X. Zhao, Carbon-nanotube-modified glassy carbon electrode for simultaneous determination of dopamine, ascorbic acid and uric acid: The effect of functional groups, Sensors and Actuators B: Chemical, 171 (2012) 1132-1140.

[37] J. Gao, W. Li, H. Shi, M. Hu, R.K.Y. Li, Preparation, morphology, and mechanical properties of carbon nanotube anchored polymer nanofiber composite, Composites Science and Technology, 92 (2014) 95-102.

[38] J. Lin, W. Wang, J. Cheng, Z. Cui, J. Si, Q. Wang, W. Chen, Modification of thermoplastic polyurethane nanofiber membranes by in situ polydopamine coating for tissue engineering, Journal of Applied Polymer Science, 137 (2020) 49252.

[39] C. Lee, L. Jug, E. Meng, High strain biocompatible polydimethylsiloxane-based conductive graphene and multiwalled carbon nanotube nanocomposite strain sensors, Applied Physics Letters, 102 (2013) 183511.

[40] J. Zhao, C. He, R. Yang, Z. Shi, M. Cheng, W. Yang, G. Xie, D. Wang, D. Shi, G. Zhang, Ultra-sensitive strain sensors based on piezoresistive nanographene films, Applied Physics Letters, 101 (2012) 063112.

[41] X.W. Zhang, Y. Pan, Q. Zheng, X.S. Yi, Time dependence of piezoresistance for the conductor‐filled polymer composites, Journal of Polymer Science part B: polymer physics, 38 (2000) 2739-2749.

[42] J.G. Simmons, Generalized formula for the electric tunnel effect between similar electrodes separated by a thin insulating film, Journal of applied physics, 34 (1963) 1793-1803.

[43] P. Sheng, E. Sichel, J.I. Gittleman, Fluctuation-induced tunneling conduction in carbon-polyvinylchloride composites, Physical Review Letters, 40 (1978) 1197.

[44] K. Yang, F. Yin, D. Xia, H. Peng, W. Yuan, A highly flexible and multifunctional strain sensor based on a network-structured MXene/polyurethane mat with ultra-high sensitivity and a broad sensing range, Nanoscale, 11 (2019) 9949-9957.

[45] X. Wang, S. Meng, M. Tebyetekerwa, Y. Li, J. Pionteck, B. Sun, Z. Qin, M. Zhu, Highly sensitive and stretchable piezoresistive strain sensor based on conductive poly (styrene-butadiene-styrene)/few layer graphene composite fiber, Composites Part A: Applied Science and Manufacturing, 105 (2018) 291-299.

[46] Y. Zhou, P. Zhan, M. Ren, G. Zheng, K. Dai, L. Mi, C. Liu, C. Shen, Significant stretchability enhancement of a crack-based strain sensor combined with high sensitivity and superior durability for motion monitoring, ACS applied materials & interfaces, 11 (2019) 7405-7414.

[47] X. Wang, H. Sun, X. Yue, Y. Yu, G. Zheng, K. Dai, C. Liu, C. Shen, A highly stretchable carbon nanotubes/thermoplastic polyurethane fiber-shaped strain sensor with porous structure for human motion monitoring, Composites Science and Technology, 168 (2018) 126-132.

[48] H. Wu, Q. Liu, H. Chen, G. Shi, C. Li, Fibrous Strain Sensor with Ultra-sensitivity, Wide Sensing Range, and Large Linearity for Full-Range Detection of Human Motion,

Nanoscale, 10 (2018) 1-9.

[49] X. Wang, X. Liu, D.W. Schubert, Highly sensitive ultrathin flexible thermoplastic polyurethane/carbon black fibrous film strain sensor with adjustable scaffold networks, Nano-Micro Letters, 13 (2021) 1-19.

[50] S. Ribeiro, P. Costa, C. Ribeiro, V. Sencadas, G. Botelho, S. Lanceros-Méndez, Electrospun styrene–butadiene–styrene elastomer copolymers for tissue engineering applications: Effect of butadiene/styrene ratio, block structure, hydrogenation and carbon nanotube loading on physical properties and cytotoxicity, Composites Part B: Engineering, 67 (2014) 30-38.

[51] S. Cantournet, R. Desmorat, J. Besson, Mullins effect and cyclic stress softening of filled elastomers by internal sliding and friction thermodynamics model, International Journal of Solids and Structures, 46 (2009) 2255-2264.

Fabrication of ultra-high working range strain sensor using carboxyl CNTs coated electrospun TPU assisted with dopamine

Yuhao Wang [1], Wenyue Li [1], Chenchen Li [1], Bangze Zhou [1], Yanfen Zhou [1], Liang Jiang [1, *], Shipeng Wen [2], Fenglei Zhou [1, 3, *]

[1] College of Textiles and Clothing, Qingdao University, Qingdao, 266071, China

[2] Beijing Engineering Research Center of Advanced Elastomers, Beijing University of Chemical Technology, Beijing 100029, China

[3] Department of Medical Physics and Biomedical Engineering, University College London, London, WC1V 6LJ, UK

Abstract

Fiber-based strain sensors have attracted widespread concern of researchers due to large specific surface area, good stretchability and remarkable flexibility. In this work, a stretchable strain sensor with ultra-high working range was developed by using electrospun thermal plastic polyurethane (TPU) nanofibrous membrane coated with carboxyl multi-walled carbon nanotubes (CNTs). In order to obtain an even distribution and an improved fastness of carboxyl CNTs on TPU fibers, dopamine (DA) was employed to modify the TPU nanofibrous membrane (labelled DATPU) via a fast ultrasonication-assisted deposition approach. DATPU/CNTs exhibited an ultra-high working range of about 710% with high gauge factor up to 1200. Furthermore, DATPU/CNTs were found to have stronger washing fastness than TPU/CNTs owing to the introduction of DA onto the surface of TPU nanofibers. DATPU/CNTs also maintained good electrical conductivity during 15000 cycles of stretching-releasing test.

[*] Corresponding authors, email address: liang.jiang@qdu.edu.cn, fenglei.zhou@ucl.ac.uk

Finally, a prototype of strain sensor based on DATPU/CNTs membrane demonstrated remarkable flexibility and sensitivity to human body motions such as elbow bending, finger bending and swallowing.

Keywords: Polyurethane nanofibers; electrospinning; dopamine modification; carbon nanotubes; strain sensor

Introduction

Recently, the demand of smart wearable electronics with the advantages of intelligence, compact size and portability has soared sharply [1-3], because they could provide great potential in human motion detection and health monitoring, etc [4-7]. One important category is strain sensors, which possess the ability of transforming the physical deformation into electrical signals [8]. An excellent strain sensor should have a wide working range, high sensitivity and good durability [9-11]. However, conventional metal-based and semiconductor-based strain sensors are subject to the stiffness, poor working range (< 5%) and low sensitivity, and therefore cannot meet the requirement of wearable device [12, 13].

Flexible strain sensors based on electrically conductive polymer fiber composites, which are composed of stretchable polymer fibers and conductive fillers or conductive layers, have been the focus of an increasing number of scientific publications because of its lightness, flexibility and stretchability [14, 15]. Stretchable polymer fibers elastomers, such as thermoplastic polyurethane (TPU) [16, 17], Ecoflex [18] and styrene butadiene styrene (SBS) [19], are generally fabricated by wet spinning [20], melt spinning [21] and electrospinning, etc. Among these, electrospinning as a simple and easy approach is usually utilized to manufacture micro/nano fibrous membrane, which possesses superiorities of large specific surface area and commendable mechanical flexibility [22]. Flexible strain sensors prepared by coating electrospun

fibrous membranes with carbon black (CB) [23], reduced graphene oxide (RGO) [24] and carbon nanotubes (CNTs) [25] have attracted increasing attention. For example, Zhao [9] et al. prepared a strain sensor by depositing CB particles onto electrospun TPU fibrous membrane assisted by ultrasonication. In order to improve the working stability of strain sensor, CB/TPU membrane was encapsulated into Ecoflex layer. The obtained CB/TPU/Ecoflex strain sensor exhibited an ultrahigh sensitivity, (i.e. the maximum gauge factor was up to 3186.4 at strain of 225%) while the working range was low (225%). In addition, Lu [26] et al. fabricated a silver nanowires (AgNWs)/TPU/polydimethylsiloxane (PDMS) sandwich structured strain sensor via sequential coating the electrospun TPU membrane with AgNWs and PDMS by filtration. The resultant strain sensor presented good stability and reliability, but was subject to low working range (about 80%) and low sensitivity (gauge factor, which refers to the sensitivity of conductive fibrous membranes to tension, was about 12). Gong [27] et al. incorporated the electrospun carbon sponge (CS) into PDMS to obtain a flexible and wearable strain sensor, which showed high piezoresistive sensibility and high-speed response. However, the working range and gauge factor (GF) of CS/PDMS strain senor was just up to 60% and 130.5, respectively. As pointed out in previous studies [28-31], a high working range could result in the reduction of materials service life in detecting high strain levels movement. Hence, there is a high-demand of electrospun fibrous membrane-based strain sensors with improved working range.

In this work, TPU electrospun fibrous membrane with excellent elasticity and toughness was selected as substrate. CNTs were selected as the conductive medium because of its very high mechanical strength and electrical conductivity. A highly stretchable strain sensor was fabricated by coating CNTs on TPU fibrous membrane assisted by ultrasonication. In order to further improve the electrical stability of the

membrane and the fastness of CNTs coated on the membrane, dopamine (DA), which was widely used to modify the surface of materials to improve the interfacial strength [32], was utilized to modify the TPU fibrous membrane (DATPU) to enhance the interfacial interactions between CNTs and TPU membrane. The influence of DA modification and the concentration of the CNTs suspension on the performance of conductive fibrous membrane were investigated. The ability of an optimized conductive fibrous membrane to detect various human body motions, such as swallow, finger bending, wrist bending and knee bending, was evaluated. Finally, a prototype strain sensor was assembled together with Bluetooth device and battery and its performance was demonstrated via detecting human kneecap motions.

Experimentation

Materials

TPU was acquired from Shandong INOV New Materials Co., Ltd. (Zibo, Shandong, China). CNTs were purchased from Cnano Technology (Beijing China). Tetrahydrofuran (THF), N, N-dimethylformamide (DMF) were bought from Sinopharm Chemical Reagent Co., Ltd. (Shanghai, China). Dopamine hydrochloride (DA·HCl) and Sodium periodate ($NaIO_4$) were obtained from Shanghai Macklin Biochemical Co., Ltd. (Shanghai, China). Tris (hydroxymethyl) aminomethane (Tris) was produced from Beijing Solarbio Science & Technology Co., Ltd. (Beijing, China). .

Preparation of electrospun TPU fibrous membrane

Figure 1(a) shows the procedure for fabricating electrospun TPU nanofibers. TPU pellets were initially desiccated in a vacuum oven at 80 °C for 24 h. Then, they were dissolved with concentration of 18 wt% in a mixed solvent of THF and DMF with a volume ratio of 3:1. The mixture was magnetically stirred at 60 °C for 8 h for complete dissolving. In order to obtain electrospun TPU fibrous membrane, TPU solution was

loaded in a plastic syringe (10 mL) connected to a 22-gauge blunt end needle which was fixed on a digital syringe pump (Longer Precision Pump Co., Ltd., Baoding, Hebei, China). Electrospinning was carried out under the room temperature, humidity of 25%, the applied voltage of 20 kV, the work distance of 20 cm between the capillary tip and the collector, and the solution supply rate of 4 mL/h. Finally, the resultant TPU fibrous membranes were placed in a fume hood overnight at room temperature to remove the remaining solvent as much as possible.

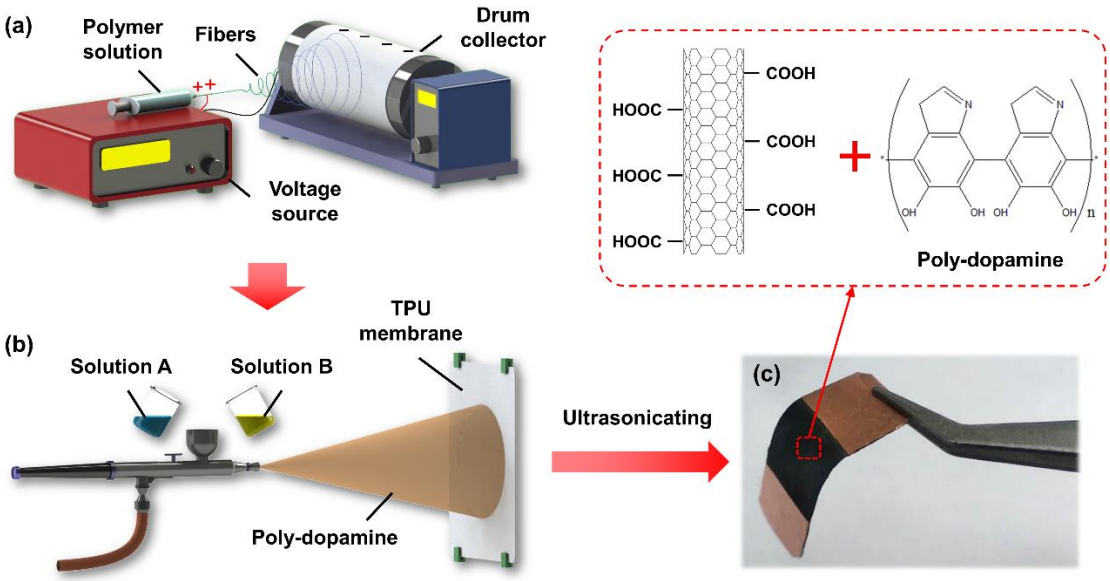

Figure 1 Schematic diagram of preparing conductive fibrous membrane: illustration of (a) fabricating TPU nanofibers and (b) DA modifying TPU nanofibers; (c) photo of DATPU/CNTs fibrous membrane.

Dopamine modification of electrospun TPU fibrous membrane

For the surface modification of electrospun TPU fibrous membrane, a 2.0 g/L aqueous solution of DA was prepared by dissolving the DA·HCl powder in distilled water and the pH of the solution was adjusted to 8.5 by adding Tris (the DA solution was termed as solution A). $NaIO_4$ aqueous solution with a concentration of 30 mM was noted as solution B. Solution A and solution B was mixed immediately and sprayed onto the TPU fibrous membrane. With the spontaneous deposition of an adherent poly-

dopamine (PDA) layer, the color of the mixture quickly changed from light pink to dark brown (Figure 1(b)). After 2 h, the TPU fibrous membrane was washed using distilled water and dried at 60 °C in a vacuum. The resultant TPU fibrous membranes were termed as DATPU.

Preparation of carboxyl CNTs

CNTs were treated by ultrasonicating in H_2SO_4/HNO_3 (3:1) mixed acid with a concentration of 10 g/L for 12 h, then stirring for 8 h at 65 °C. The mixture of carboxyl CNTs was centrifuged at 6000 r/min for 20 min and filtered through 0.22 μm filter paper. The modified CNTs were then washed to neutral with distilled water and dried in a vacuum at 40 °C. Detailed description of CNTs and carboxyl CNTs characterization was presented in the previous work [3]. Carboxyl CNTs were employed in the following work, which is also called CNTs in convenience.

Preparation of CNTs coated TPU fibrous membrane

Firstly, CNTs was added into distilled water to prepare the CNTs suspension with the concentration of 0.2 g/L, 0.4 g/L, 0.6 g/L, 0.8 g/L and 1.0 g/L. Both pure TPU and DATPU fibrous membranes with the size of 40 mm×10 mm were soaked into the above CNTs suspension. After ultrasonication for 60 min, the CNTs coated pure TPU and DATPU fibrous membrane were removed from the beaker, washed with distilled water for three times and placed in a vacuum oven at 60 °C for 24 h. The CNTs coated pure TPU and DATPU fibrous membranes were termed as TPU/CNTs-X and DATPU/CNTs-X, respectively (X means the concentration of CNTs suspension).

Characterization

The morphology of the samples was observed by using a scanning electron microscope (SEM) (Hitachi Regulus 8100, Tokyo, Japan).

Electrical sheet resistance of TPU/CNTs and DATPU/CNTs conductive fibrous

membrane was measured by using a multifunction digital four-probe tester (ST-2258C, Jiangsu, China).

Tensile tests were carried out by using a tensile testing machine (Instron-5965 Tensile Machine, Glenview, US) with the stretch rate of 100 mm/min. Rectangular specimens with the size of 40 mm×10 mm were used, and the clamping distance was 20 mm.

The surface chemical structure of the sample was carried out using X-ray photoelectron spectroscopy (XPS) (Thermo ESCALAB 250XI system Thermo Electron Corporation, USA) with an Al Kα X-ray source.

Thermogravimetric analysis (TGA) was performed using a DSC/TG synchronous thermal analyzer (STA449 F3 Jupiter, Bavaria, Germany) under nitrogen atmosphere. The sample, with a weight of 5-10 mg, was heated from room temperature to 800 °C with a heating rate of 20 °C/min.

The resistance of TPU/CNTs and DATPU/CNTs conductive fibrous membrane was measured with a digital multimeter (KEYSIGHT B2901A, US) which was equipped with a stepper motor to induce various tensile deformations in the tested samples.

Results and discussion

In this work, concentration of the CNTs suspension is a key factor in fabricating a conductive fibrous membrane with excellent conductivity. Therefore, CNTs suspension concentration was varied from 0.2 g/L, 0.4 g/L, 0.6 g/L, 0.8 g/L to 1.0 g/L to investigate its effect on the morphology, thermal properties and mechanical properties of conductive fibrous membrane. The morphology of resultant conductive fibrous membranes is depicted in Figure 2. As shown in Figure 2(a-f), the TPU fibers exhibited relatively smooth surface before ultrasonicating. As the concentration of CNTs suspension increased, there were more CNTs coated on the TPU fibers. However, by comparison with the pure TPU fibers, DATPU fibers possessed rougher surface, which

should be ascribed to the self-polymerization of DA on the surface of the TPU fiber, forming a poly-dopamine layer. Besides, DATPU fibrous membranes appeared to bind with more CNTs than TPU fibrous membrane for the same concentration of CNTs suspension.

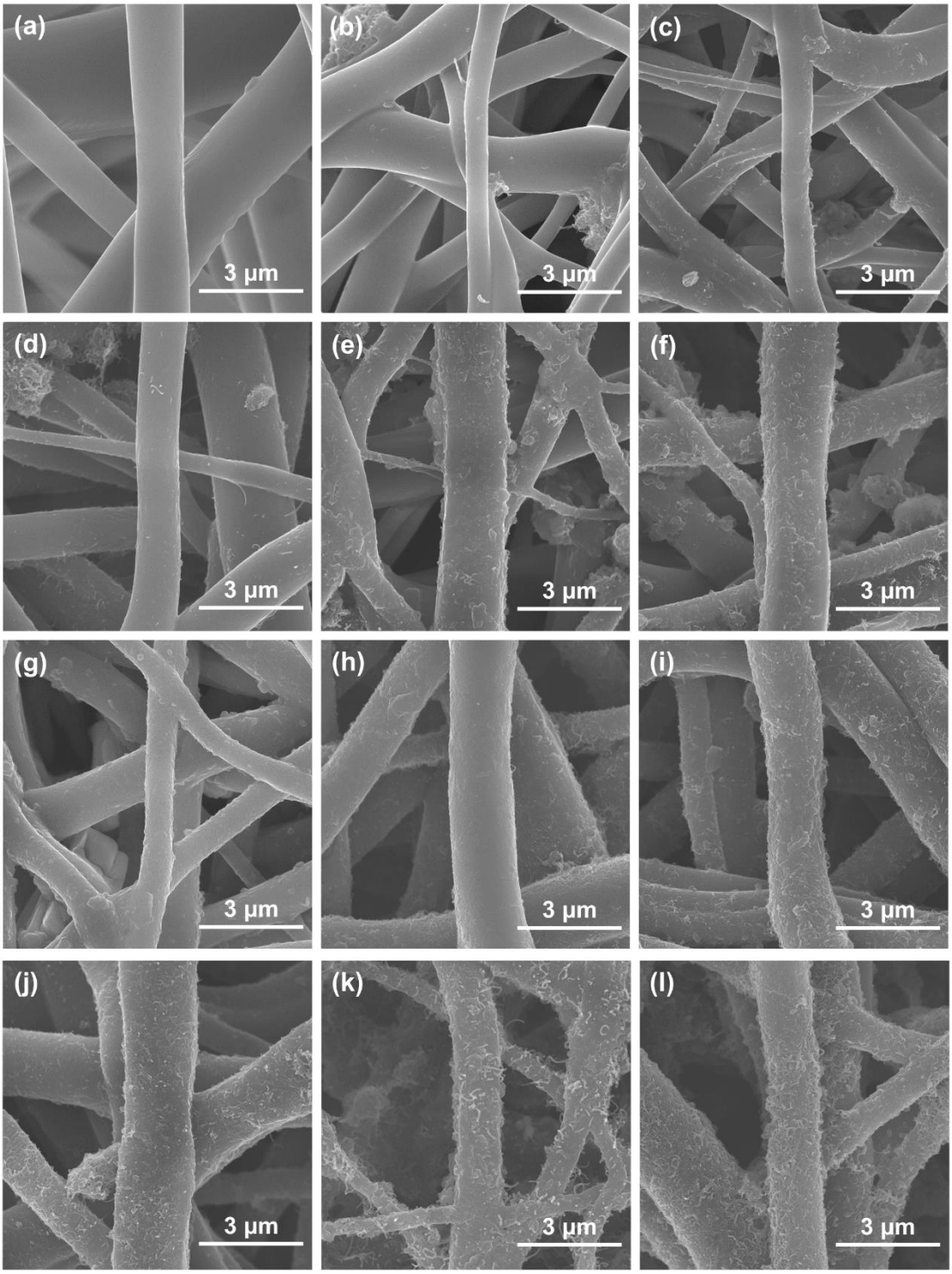

Figure 2 Morphology of (a) pure TPU; (b) TPU/CNTs-0.2; (c) TPU/CNTs-0.4; (d) TPU/CNTs-0.6; (e) TPU/CNTs-0.8; (f) TPU/CNTs-1.0; (g) DATPU; (h) DATPU/CNTs-0.2; (i) DATPU/CNTs-0.4; (j) DATPU/CNTs-0.6; (k) DATPU/CNTs-0.8; (l) DATPU/CNTs-1.0.

TGA was performed to determine the amount of CNTs coated on the fibrous membrane. As is shown in the Figure 3(a) and (c), when the temperature reached 800 °C, mass residue of pure TPU was about 8.93%, and the mass residues of TPU/CNTs-0.2, TPU/CNTs-0.4, TPU/CNTs-0.6, TPU/CNTs-0.8 and TPU/CNTs-1.0 were about 10.36%, 12.08%, 12.90%, 14.53% and 16.43%, which indicated that the content of CNTs coated on the TPU fibrous membranes were 1.57% (TPU/CNTs-0.2), 3.46% (TPU/CNTs-0.4), 4.36% (TPU/CNTs-0.6), 6.15% (TPU/CNTs-0.8) and 8.24% (TPU/CNTs-1.0), respectively. In contrast, for the TPU fibrous membranes modified with DA, the amount of CNTs on the DATPU fibrous membranes were about 3.31%, 5.67%, 7.13%, 8.76% and 9.79%, correspondingly. As is shown in Figure 3(b) and (d), the sheet resistance of the conductive membranes was inversely proportional to the content of CNTs coated. The sheet resistance of TPU/CNTs membranes decreased from 151.66±45.44 kΩ/sq to 0.65±0.14 kΩ/sq when the concentration of CNTs suspension increased from 0.2 g/L to 1.0 g/L. After being modified by DA, DATPU/CNTs offered a decrease of sheet resistance from 14.38±2.56 kΩ/sq to 0.32±0.11 kΩ/sq when the concentration of CNTs suspension increased from 0.2 g/L to 1.0 g/L. Notably, DATPU/CNTs exhibited lower sheet resistance than TPU/CNTs for the same concentration of CNTs suspension used. The results of the morphology proved that DATPU had a better ability to bind with CNTs, and the resultant conductive membranes possessed higher electrical conductivity. The relative higher amount of CNTs on

DATPU than TPU fibres should be responsible for the increase in electrical conductivity of DATPU/CNTs composites.

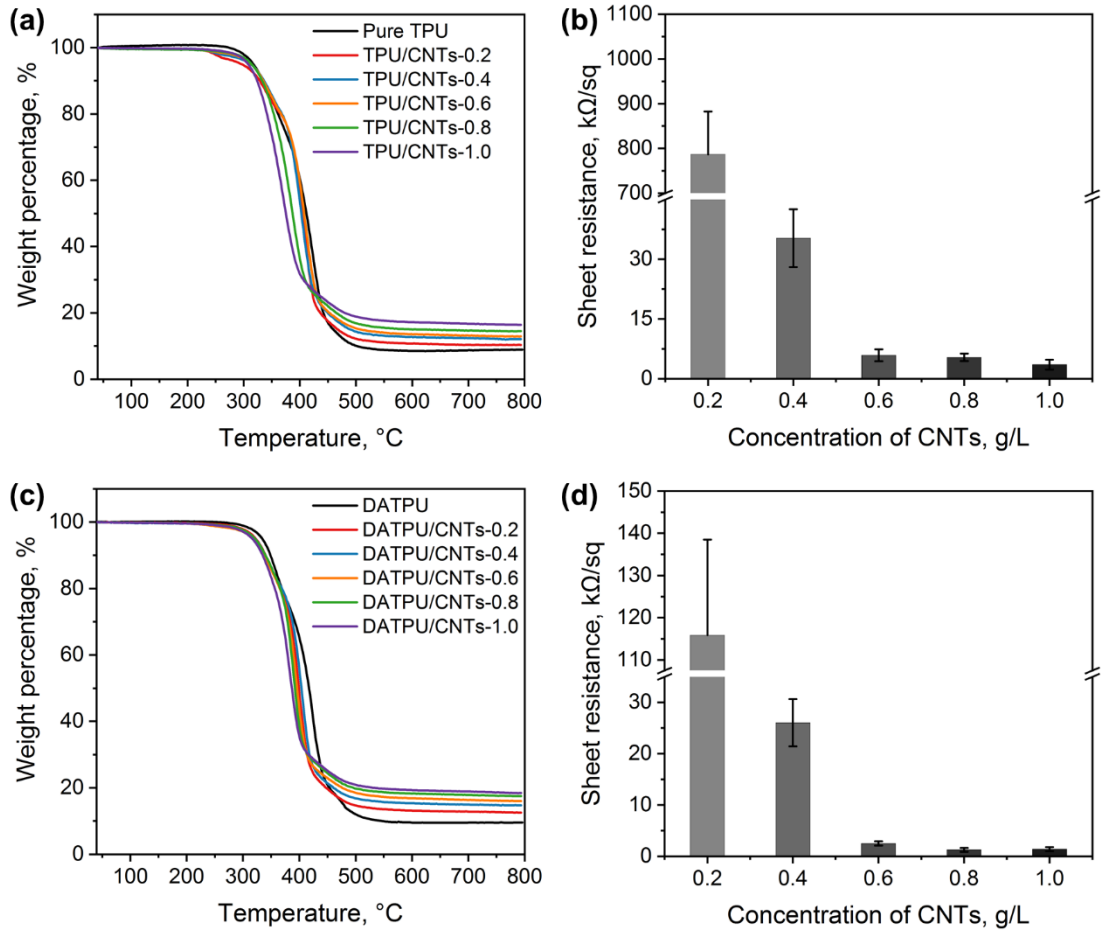

Figure 3 (a) TGA curves of pure TPU and TPU/CNTs fabricated using different CNTs suspension; (b) Histogram of sheet resistance of the TPU/CNTs fabricated using CNTs suspension with different concentration; (c) TGA curves of DATPU and DATPU/CNTs fabricated using CNTs suspension with different concentration; (d) Histogram of sheet resistance of the DATPU/CNTs fabricated using CNTs suspension with different concentration.

XPS spectra are demonstrated in Figure 4. As seen from the wide scan spectra of pure TPU and DATPU (Figure 4(a) and (b)), the peaks of C 1s, O 1s and N 1s were at 284.8 eV, 530.9 eV and 400.5 eV, respectively. From the C 1s core level spectrum of TPU shown in the Figure 4(c), one peak at 284.8 eV referred to the C-H/C-C groups, one

peak at 286.5 eV was related to C-O groups and another peak at 288.9 eV was attributed to NH-COO groups [33]. After coated with CNTs, there was a peak emerging at 283.6 eV referred to CNTs together with the other three peaks of C-H/C-C, C-O and NH-COO curve-fitting the C 1s core level spectrum of TPU/CNTs, as shown in Figure 4(d). As can been observed from Figure 4(e), a new peak of C-N at 285.3 eV in C 1s core level spectrum of DATPU appeared in comparison with pure TPU, indicating that the TPU fibrous membrane was modified by dopamine successfully [34]. The C 1s core level spectrum of DATPU/CNTs is exhibited in Figure 4(f), from which it can be seen that the peak of CNTs shifted to higher binding energy of 284.2 eV compared to that of TPU/CNTs. This is mainly due to the strong hydrogen bond between hydroxyl group and amino group on dopamine and the carboxyl group on the CNTs, resulting in that the carboxyl group becomes more electropositive [35]. Furthermore, because the dopamine and the -COOH group existed as cations and anions, respectively, it led to strong interactions between the CNTs and DATPU fibrous membrane [36]. In summary, the experimental results mentioned above confirmed that DA layer could bond the TPU fibers with CNTs tightly, resulting in an improved quantity of the CNTs coated on the DATPU and thus the conductivity of DATPU/CNTs remarkably.

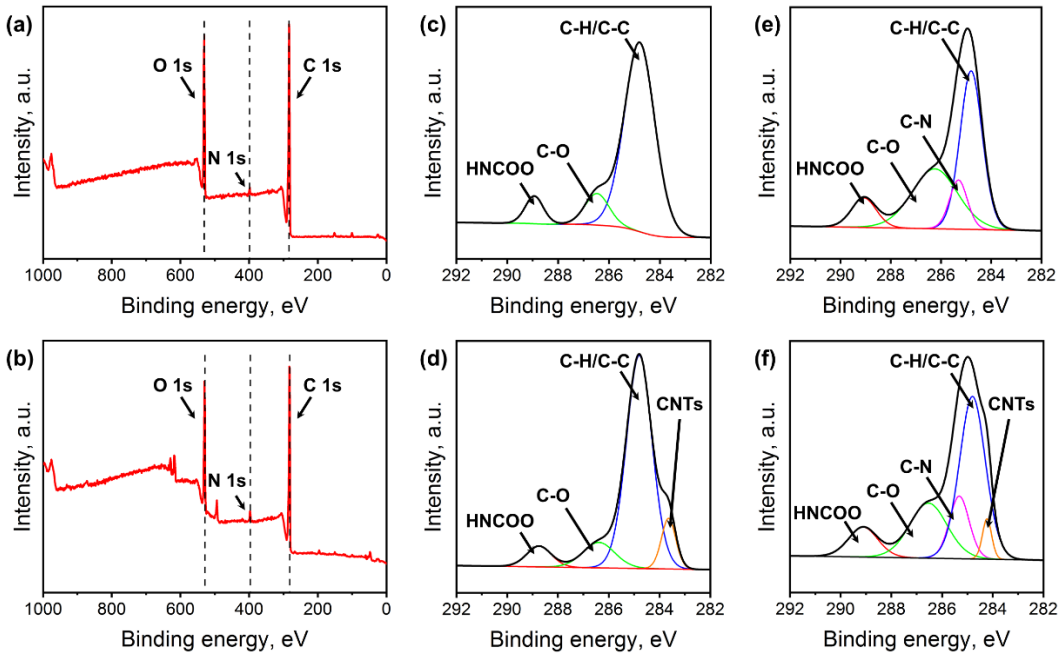

Figure 4 XPS wide scan spectra of (a) pure TPU and (b) DATPU; C 1s core level spectrum of (c) pure TPU; (d) TPU/CNTs; (e) DATPU; (f) DATPU/CNTs.

Mechanical properties are the crucial indicators for evaluating materials in practical applications. The typical stress-strain curves of conductive composite fibrous membranes are shown in Figure 5. It can be seen from the Figure 5 and Table 1 that the tensile strength of the conductive fibrous membrane increased with increasing concentration of CNTs suspension for both TPU and DATPU nanofibers. For example, the TPU/CNTs-1.0 possessed a tensile strength of 11.15±0.12 MPa, which was about 2.80 MPa higher than pure TPU, while the tensile strength of DATPU/CNTs-1.0 was 11.75±0.15 MPa, which was about 3.19 MPa higher than DATPU. This obviously enhanced tensile strength might benefit from the significant reinforce effect of CNTs [37]. In addition, as mentioned previously in this study, DA coating layer, which has a strong interaction with TPU fibers, could led to a higher tensile strength of DATPU (8.56±0.33 MPa) than that of pure TPU (8.35±0.21 MPa) [38]. Owing to the amount of CNTs coated on DATPU was higher than that of TPU, DATPU/CNTs fibrous membranes exhibited higher tensile strength than TPU/CNTs. However, the elongation

at break slightly decreased from 1043±39% to 934±30% after the TPU fibrous membranes were modified via DA, as shown in Figure 5b. This might be because that DA layer as well as the CNTs interconnected the fibers, facilitating a decreasing slippage of between fibers [11]. Due to the excellent electrical conductivity and mechanical property, the conductive DATPU/CNTs fibrous membrane- prepared using 1.0 g/L of CNTs suspension were chosen for further investigation on the electromechanical properties. For convenience of reading, TPU/CNTs-1.0 and DATPU/CNTs-1.0 are abbreviated as TPU/CNTs and DATPU/CNTs respectively in the following.

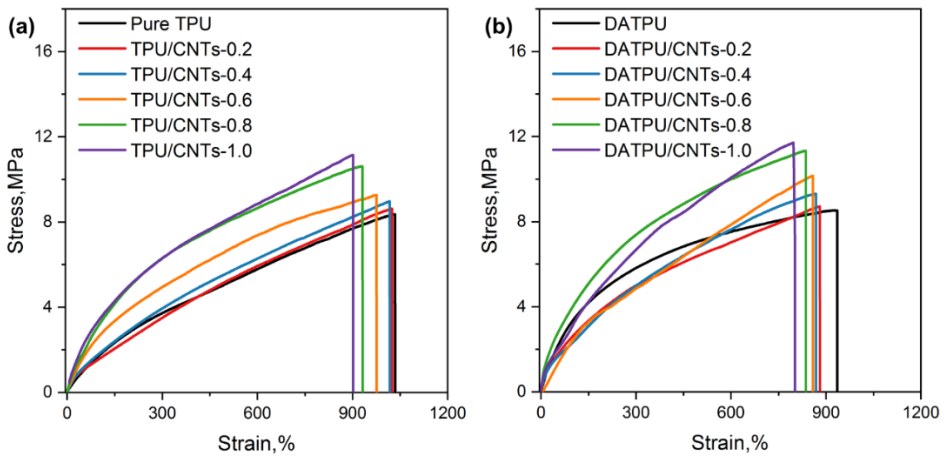

Figure 5 Strain-stress curves of (a) pure TPU and TPU/CNTs fabricated using different CNTs suspension; (b) DATPU and DATPU/CNTs fabricated using different CNTs suspension.

Table 1 Mechanical properties: tensile strength (σ) and elongation at break ($\varepsilon_{at\ break}$)

Sample	σ (MPa)	$\varepsilon_{at\ break}$ (%)	Sample	σ (MPa)	$\varepsilon_{at\ break}$ (%)
Pure TPU	8.35±0.21	1043±39	DATPU	8.56±0.33	934±30
TPU/CNTs-0.2	8.63±0.17	1025±18	DATPU/CNTs-0.2	8.75±0.11	889±25
TPU/CNTs-0.4	8.96±0.20	1014±16	DATPU/CNTs-0.4	9.37±0.16	866±34
TPU/CNTs-0.6	9.25±0.23	982±18	DATPU/CNTs-0.6	10.16±0.16	852±40
TPU/CNTs-0.8	10.62±0.19	934±33	DATPU/CNTs-0.8	11.38±0.35	832±27
TPU/CNTs-1.0	11.15±0.12	903±29	DATPU/CNTs-1.0	11.75±0.15	807±27

In this work, the electrical properties such as relative resistance ($\Delta R/R_0$, $\Delta R=R-R_0$, R is the real-time resistance, R_0 represents the original resistance) and gauge factor (GF) (($\Delta R/R_0$)/ε, ε is the strain) were characterized. The gauge factor was defined as the ratio of the change of relative resistance to the change of strain. As shown in Figure 6(a) and (b), the TPU/CNTs membrane exhibited a wide working range of 560% with a high GF of 130. In contrast, DATPU/CNTs possessed a larger working range of 710% (as shown in Figure 6 (d)), which was 1.5 times larger than that of TPU/CNTs. For the sensitivity, the DATPU/CNTs exhibited a GF as high as 1200, which was 9 times higher than that of TPU/CNTs (Figure 6(e)). The *I-V* curves of the TPU/CNTs and DATPU/CNTs acquired under the strain of 0%, 50%, 100%, 200%, 400% and 600%, are shown in Figure 6(c) and (f). The *I-V* curves for TPU/CNTs membranes and DATPU/CNTs membranes in the strain range from 0% to 400% were linear, indicating an excellent conductivity. When the strain exceeded 600%, the nonlinear *I-V* curve of TPU/CNTs indicated poor conductivity, while the linear *I-V* curve of DATPU/CNTs proved good conductivity.

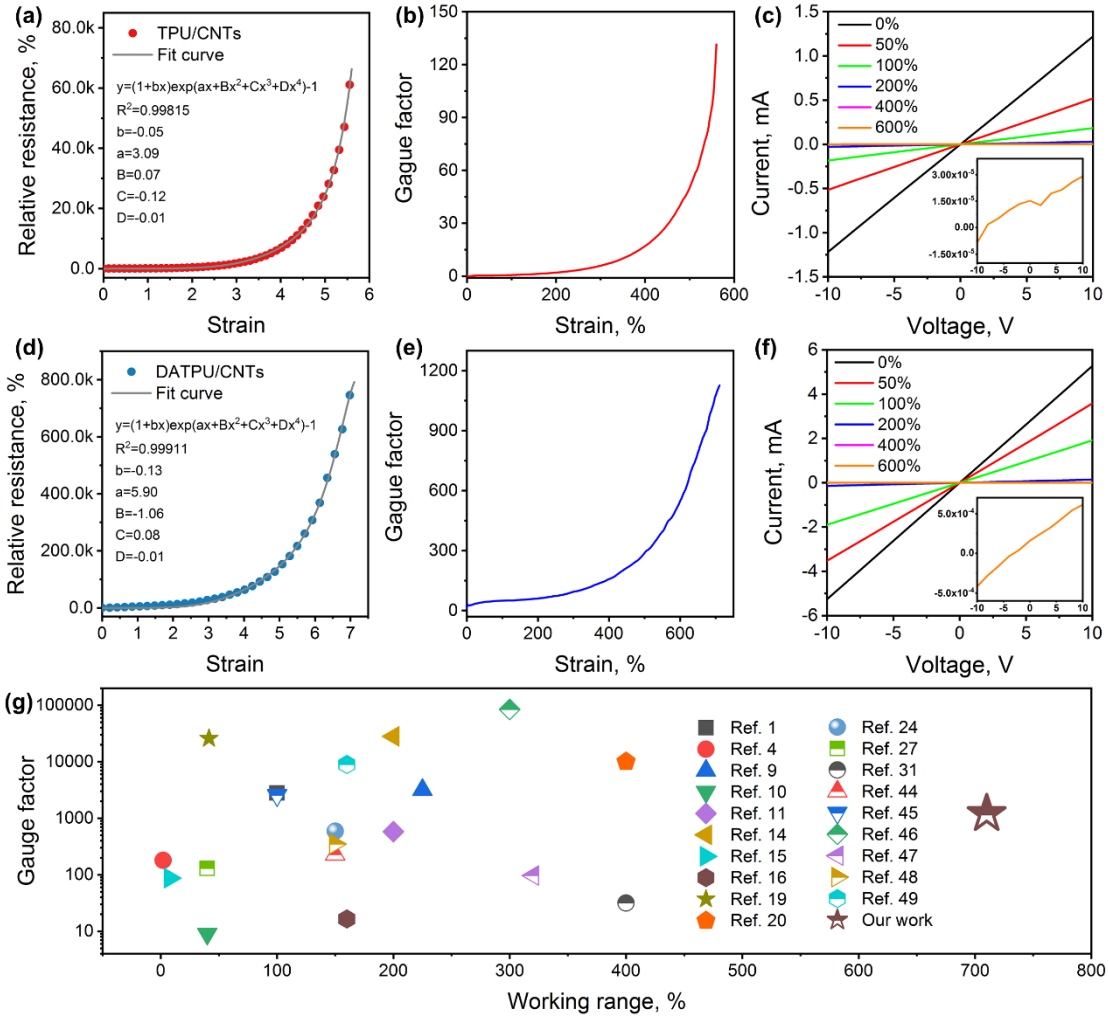

Figure 6 (a) The relative resistance-strain fitting curve of TPU/CNTs; (b) The guage factor (GF) versus strain curve of TPU/CNTs; (c) I-V curves under different applied strain of TPU/CNTs; (d) The relative resistance-strain fitting curve of DATPU/CNTs; (e) The gauge factor (GF) versus strain curve of DATPU/CNTs; (f) I-V curves under different applied strain of DATPU/CNTs; (g) comparison of the GF and the maximum working range reported between the references and our work.

As shown in Figure 6(a) and (d), the experimental data of relative resistance related to strain was fitted theoretically according to the "tunnel effect" [39, 40], whose model reported that the total electrical resistance *R* of the conductive polymer can be determined by Equation (1) and (2) below [41, 42].

$$R = \left(\frac{L}{N}\right)\left(\frac{8\pi hs}{3\gamma a^2 e^2}\right)\exp(\gamma s) \quad (1)$$

$$\gamma = \frac{4\pi\sqrt{2m\varphi}}{h} \quad (2)$$

where N refers to the number of conductive paths, L is related to the number of particles forming a conductive path, h is the Plank constant, s represents the smallest distance between the CNTs, a^2 represents the effective cross section and e is about the electron change, respectively. Besides, in the Equation (2), m is the electron mass and φ is related to the height of potential barrier between adjacent CNTs.

As the strain is applied to the conductive fibrous membranes, the resistance would increase owing to the damage of CNTs conductive networks. It can be assumed that the distance between CNTs varies from s_0 (original distance between CNTs) to s under the external force and the quantity of conductive paths decreased from N_0 (the quantity of conductive paths in the original state) to N, s and N can be calculated according Equation (3) and (4) [43].

$$s = s_0(1+b\varepsilon) \quad (3)$$

$$N = \frac{N_0}{\exp\left(A\varepsilon + B\varepsilon^2 + C\varepsilon^3 + D\varepsilon^4\right)} \quad (4)$$

where b, A, B, C, D are constant. Substituting Equation (3) and (4) into Equation (1), it can be obtained that:

$$\frac{\Delta R}{R_0} = \frac{R - R_0}{R_0} = \left(\frac{sN_0}{Ns_0}\right)\exp\left[\gamma\left(s - s_0\right)\right] - 1 = \left(1+b\varepsilon\right)\exp\left[\left(A + \gamma b s_0\right)\varepsilon + B\varepsilon^2 + C\varepsilon^3 + D\varepsilon^4\right] - 1 \quad (5)$$

As presented in Figure 6(a) and (d), the experimental data of both TPU/CNTs and DATPU/CNTs are in good agreement with the theoretical values calculated from Equations (5) with R^2 value of 0.99815 and 0.99911, respectively. As shown in the Figure 6(g), compared with the strain sensors reported in previous work [1, 4, 9-11, 14-

16, 19, 20, 24, 27, 31, 44-49], the integration of ultra-high working range and high GF leads DATPU/CNTs strain sensor to stand out, indicating a feasibility of its application in monitoring large strains.

In order to determine the fastness of CNTs coated on the fibrous membranes, DATPU/CNTs were immersed in distilled water and ultrasonicated for 20 min, 40 min, 60 min and 80 min. The morphology, TG analysis and sheet resistance of the samples after washing are shown in Figure 7. It can be seen from the SEM image that after washing for 80 min, the quantity of CNTs coating on TPU decreased considerably (Figure 7(a)), which could be caused by the removal of some CNTs during ultrasonication. In contrast, there were still a large amount of CNTs adhering to the DATPU fibrous membrane after washing for 80 min, which should be due to the strong binding between CNTs and DATPU fibers. The weight loss determined from TG analysis of TPU/CNTs after washing for 20 min, 40 min, 60 min and 80 min (as shown in Figure 7 (c)) was 86.58%, 87.62%, 88.86% and 89.47%, corresponding to the loss content of CNTs after washing of 3.31%, 4.45%, 5.81% and 6.48%, respectively. In the case of the DATPU/CNTs, the content of CNTs washed away after ultrasonicating for 20 min, 40 min, 60 min and 80 min was 1.66%, 2.47%, 3.31% and 4.04%, which were about 50% less than those TPU/CNTs samples washed the same time. Besides, the sheet resistance of TPU/CNTs increased from 5.36±0.95 kΩ/sq to 102.83±7.51kΩ/sq, while the sheet resistance of DATPU/CNTs only increased from 1.25±0.36 kΩ/sq to 15.67±3.66 kΩ/sq after washing for 80 min. These results revealed that the adhesion between DATPU fibrous membranes and CNTs was stronger than TPU fibrous membranes and CNTs.

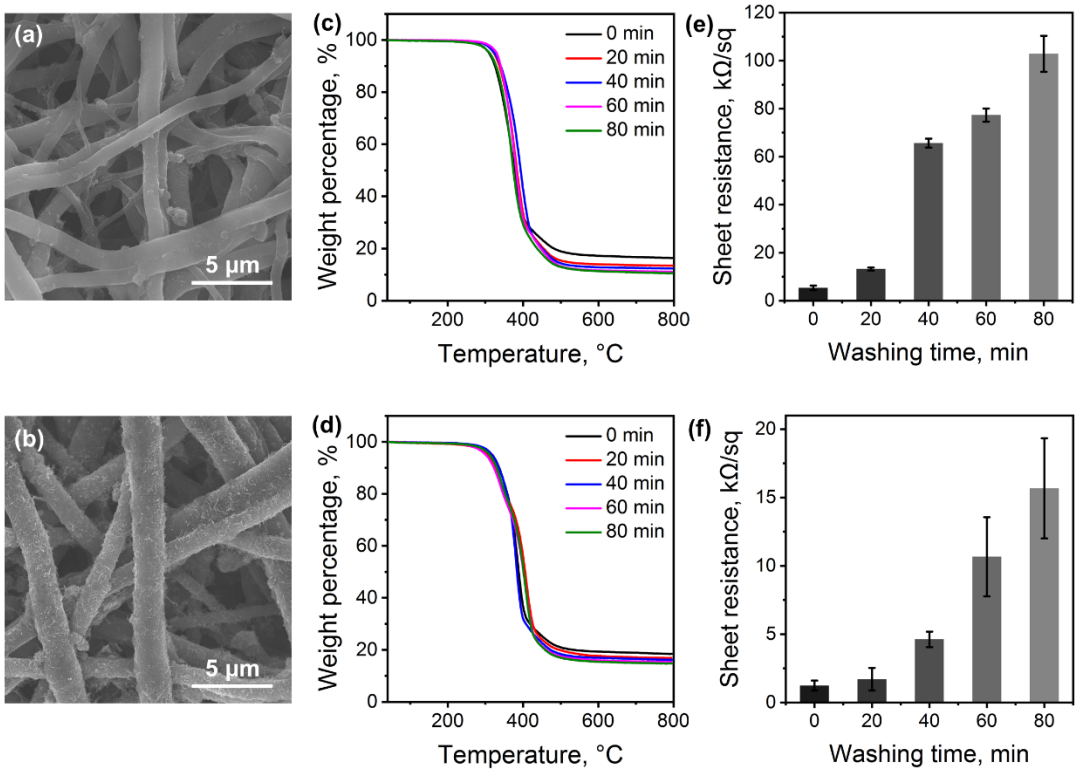

Figure 7 Morphology of (a) TPU/CNTs and (b) DATPU/CNTs after washing for 80 min; TGA curves of (c) TPU/CNTs and (d) DATPU/CNTs after washing for different time; Histogram of the sheet resistance of (e) TPU/CNTs and (f) DATPU/CNTs after washing for different time.

Figure 8 displays the sensing behavior of DATPU/CNTs at different strain ranging from 0 to 50%, 100%, 200%, 400% and 600%. It can be seen that the DATPU/CNTs conductive fibrous membrane exhibited the ability to maintain its electrical conductivity across all strain ranges. However, it should be noted that during the first four stretching-releasing cycles, the values of relative resistance did not reach a steady state, and then became constant gradually with the increasing stretching-releasing cycle number. The reason behind this can be explained from the following two aspects: the hysteresis and changes of conductive path [28] in the stretching-releasing process. As shown in Figure 8(b) and (c), when applying 50%, 100%, 200%, 400% and 600% strain of stretching-releasing to the DATPU/CNTs fibrous membranes, the mechanical

hysteresis, which was calculated according to the integration of stretching-releasing curve in each cycle, decreased obviously at the first cycle for all of the strain degrees, when the cycle number exceeded 3, the mechanical hysteresis kept stable basically. For example, under the stretching-releasing test in the strain range from 0 to 600%, the mechanical hysteresis at the first cycle was 31.87 MJ/m^3 and then decreased sharply to 4.85 MJ/m^3 at the 2^{nd} cycle and eventually remained at around 3.00 MJ/m^3 from the 3^{rd} cycle. This should be ascribed to the Mullins effect, the broken of some weak polymer chains led to a decreased number of polymer chains maintained stress. Besides, DATPU fibers macromolecular network and DATPU fibrous network rearranged, conducting to stress decreasing [50, 51].

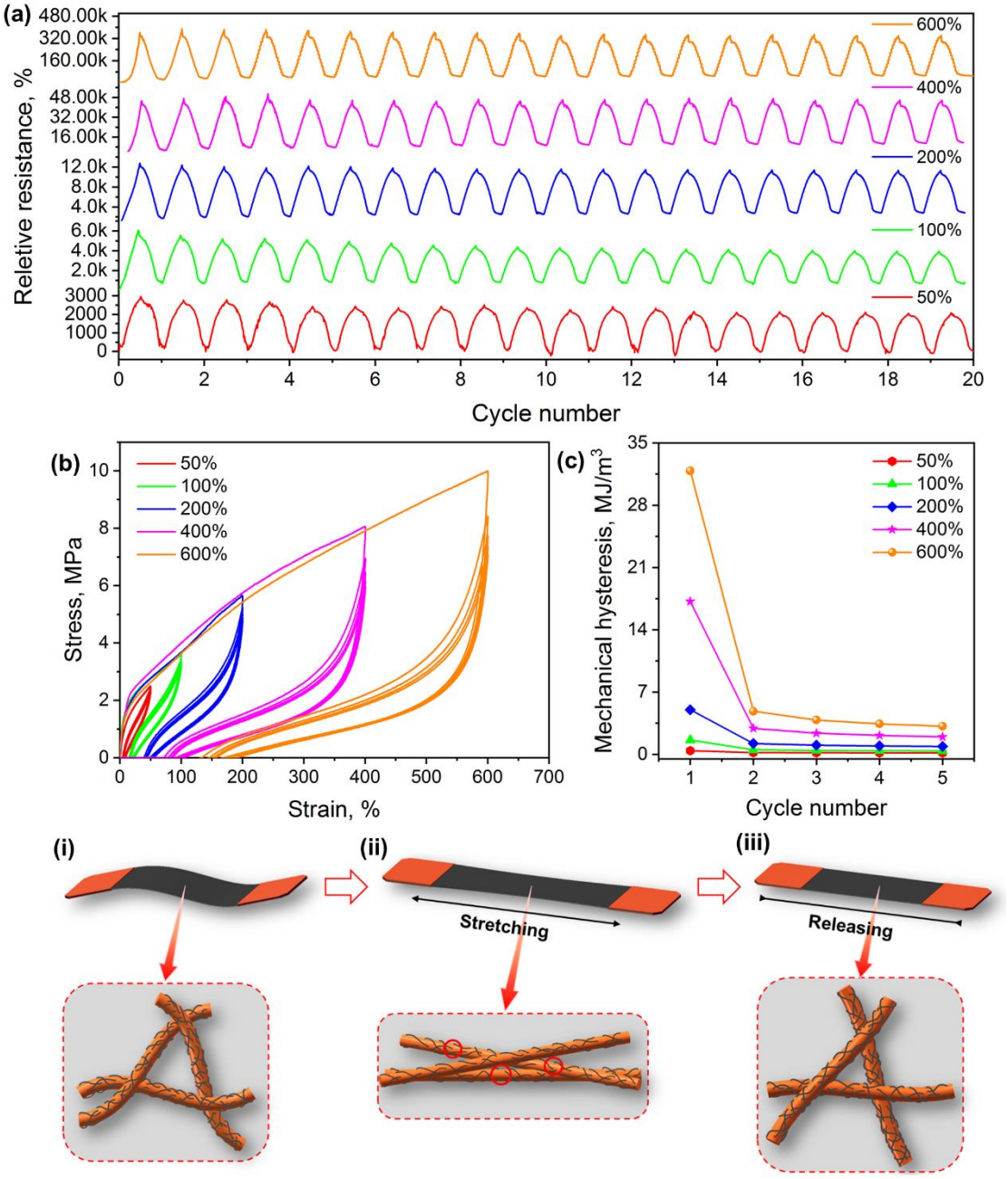

Figure 8 (a) curves of relative resistance related to 20 cycles of stretching-releasing test applied over different strain ranges: 0-50%, 0-100%, 0-200%, 0-400% and 0-600% with a constant stretching rate of 10 mm/min; (b) elastic recovery curves for five cycles stretching-releasing test of DATPU/CNTs with strain of 0-50%, 0-100%, 0-200%, 0-400% and 0-600%; (c) mechanical hysteresis of elastic recovery for DATPU/CNTs with strains of 50%-600%; schematic of the CNTs conductive network in the (i) original stage; (ii) stretching stage; (iii) releasing stage.

The schematic describing the change in CNTs conductive network in one cycle of stretching-releasing test is shown in Figure 8(i-iii). Figure 8(i) exhibits the original CNTs conductive network before stretching, which was relatively compact. Then, some of the conductive pathways were broken after stretching was applied to DATPU/CNTs (shown in Figure 8(ii)), leading to an increasing electrical resistance. However, when the stretching was released (shown in Figure 8(iii)), the conductive network could reconstruct. Therefore, the proposed break-connection of the conductive pathways upon stretching-releasing could result in relatively large variations in the value of relative resistance observed in the first few stretching-releasing tests, while once the conductive pathways were adapted to the applied stretching-releasing process, the variation in the value of relative resistance became constant with increasing the number of stretching-releasing cycles.

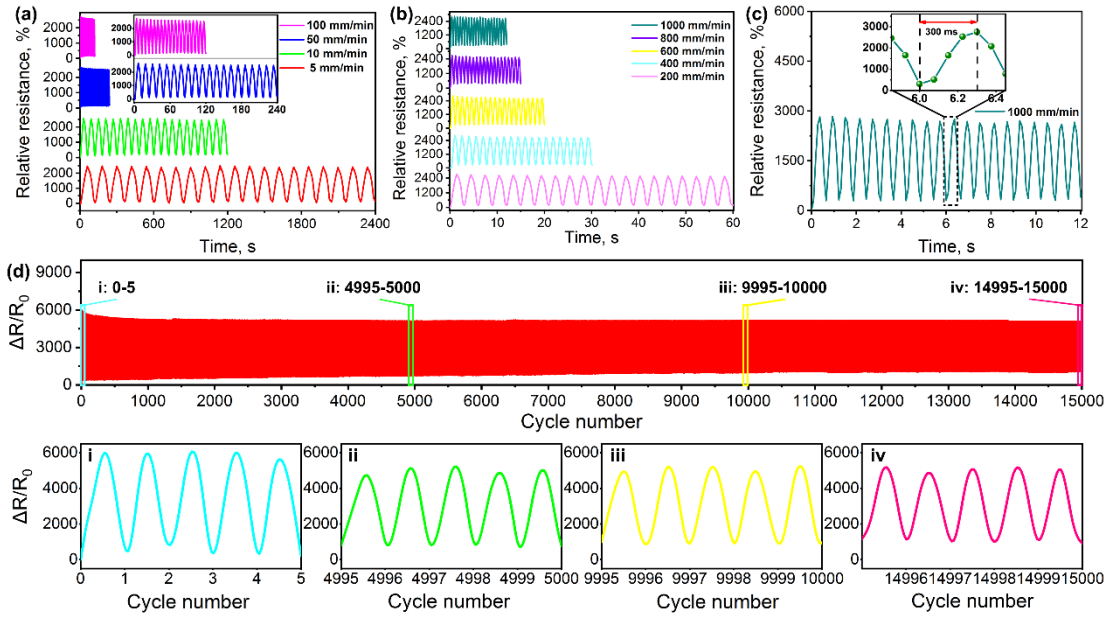

Figure 9 (a-b) curves of relative resistance under 50% strain at the stretch rate of 5 mm/min, 10 mm/min, 50 mm/min, 100 mm/min, 200 mm/min, 400 mm/min, 600 mm/min, 800 mm/min and 1000 mm/min for 20 cycles of stretching-releasing test; (c) response time for 50% abrupt strain; (d) working durability under 100% of strain for

15000 cycles of stretching-releasing test. (i-iv) show the sensing behavior in 0-5, 4995-5000, 9995-10000 and 14995-15000 cycles, respectively.

The sensing behavior of DATPU/CNTs under the stretching rates of 5 mm/min, 10 mm/min, 50 mm/min, 100 mm/min, 200 mm/min, 400 mm/min, 600 mm/min, 800 mm/min and 1000 mm/min was performed and illustrated in Figure 9(a) and (b). As can be seen from these two figures, no obvious changes in relative resistance were presented at each stretching rate, indicating that DATPU/CNTs had excellent ability to sense different external stimuli across all stretching rates. In particular, as can be seen from Figure 9(c), the strain sensor had a rapid response time of 300 ms to the abrupt strain sweep up to 50% by applying a stretch rate of 1000 mm/min. Moreover, as shown in Figure 9(d), 15000 cycles of stretching-releasing test were performed under 100% of strain and 100 mm/min of stretch rate, revealing a good durability of electrical resistance. For instance, the relative resistance was about 300% in the first 5 cycles, about 240% in 4995-5000 cycles, and remained about 240% in the following 9995-10000 and 14995-15000 cycles, revealing a good working stability of DATPU/CNTs based strain sensor.

The DATPU/CNTs composite conductive fibrous membrane was used for human motions detection in this work due to the advantages of high working range, good sensitivity, excellent stability and outstanding durability. DATPU/CNTs was fixed on the Adam's apple, fingers, wrist and knee of a volunteer, who had read and signed the consent form. As shown in Figure 10(a-d), from a tiny swallow movement (Figure 10(a)), a small finger bending movement (Figure 10(b)), through a middle wrist bending movement (Figure 10(c)) to a large knee bending movement (Figure 10(d)), the DATPU/CNTs showed high and repeatable sensitivity to these motions in the testing cycles. Besides, the response of DATPU/CNTs was found to vary the degree of

bending. For example, as the finger bending changed from 0° through 45° to 90°, the value of relative resistance changed by about 2000% and 3500%, respectively. Figure 10(i-iv) exhibits the gradual decrease in brightness of a light emitting diode (LED) with the increasing stretching up to 200% of the DATPU/CNTs membrane that was connected into an electric circuit (see Movie S1), revealing that the electrical resistance of DATPU/CNTs increased with increasing strain.

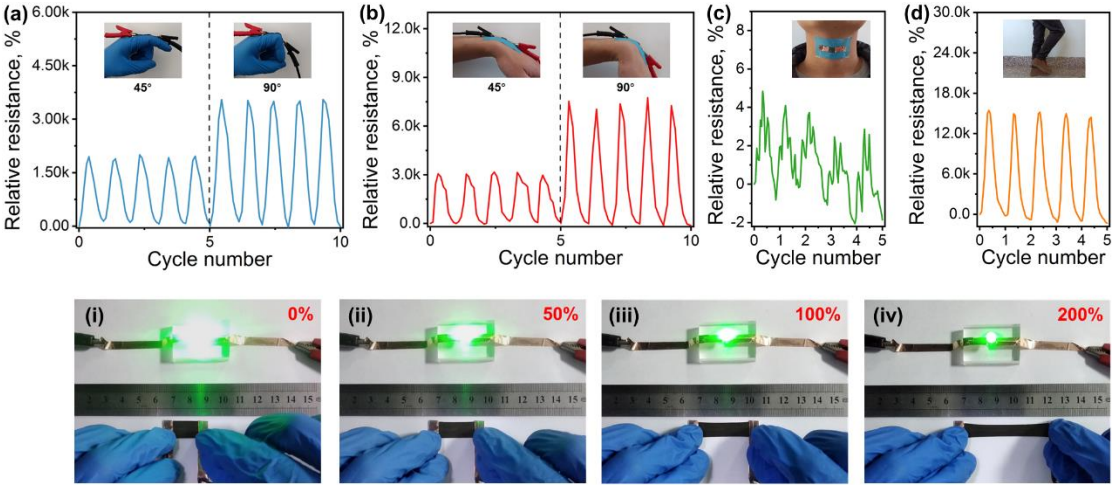

Figure 10 (a) Relative resistance obtain in real time from the human motion (a) figure bending; (b) wrist bending; (c) swallow; (d) knee bending; The brightness of LED changed with the DATPU/CNTs strain sensor stretched from (i) 0% to (ii) 50%; (iii) 100%; (iv) 200%.

A smart motion detection prototype kneecap was constructed by integrating the DATPU/CNTs strain sensor, Bluetooth device and battery. The diagram of the smart kneecap device and its main hardware components and photo are shown in Figure 11(a-b). The current signals generated from the volunteer's knee motions could be transmitted to the smart phone in real time by the Bluetooth device in the smart kneecap. The practical working condition of the smart motion detection kneecap is shown in Figure 11(c-h) and the supplementary Movie S2. At the original stage (Figure 11 (c)), a constant current signal (80 mA) was detected on the right knee of the standing-straight

volunteer, while a regularly variable current signal (about -20 mA) was seen on the right knee with a fixed bending of about 100° (Figure 11(d)). As shown in Figure 11(e and f), when the volunteer was walking (40 steps/min) and running (80 steps/min), the frequency of current signal changed corresponding to the changes in the variable knee bending frequency. In addition, as shown in Figure 11(g), the smart motion detection kneecap had a good response to human squatting movement (100° bending angle for -20 mA current change). Finally, when the human movement stopped (ending stage shown in Figure (h)), the current signal value (77 mA) returned to the same current value to the initial stage, which further confirmed the stability of the smart motion detection kneepad. These results indicated that the developed smart motion detection kneecap can sensitively and repeatedly respond to the different movements of human body.

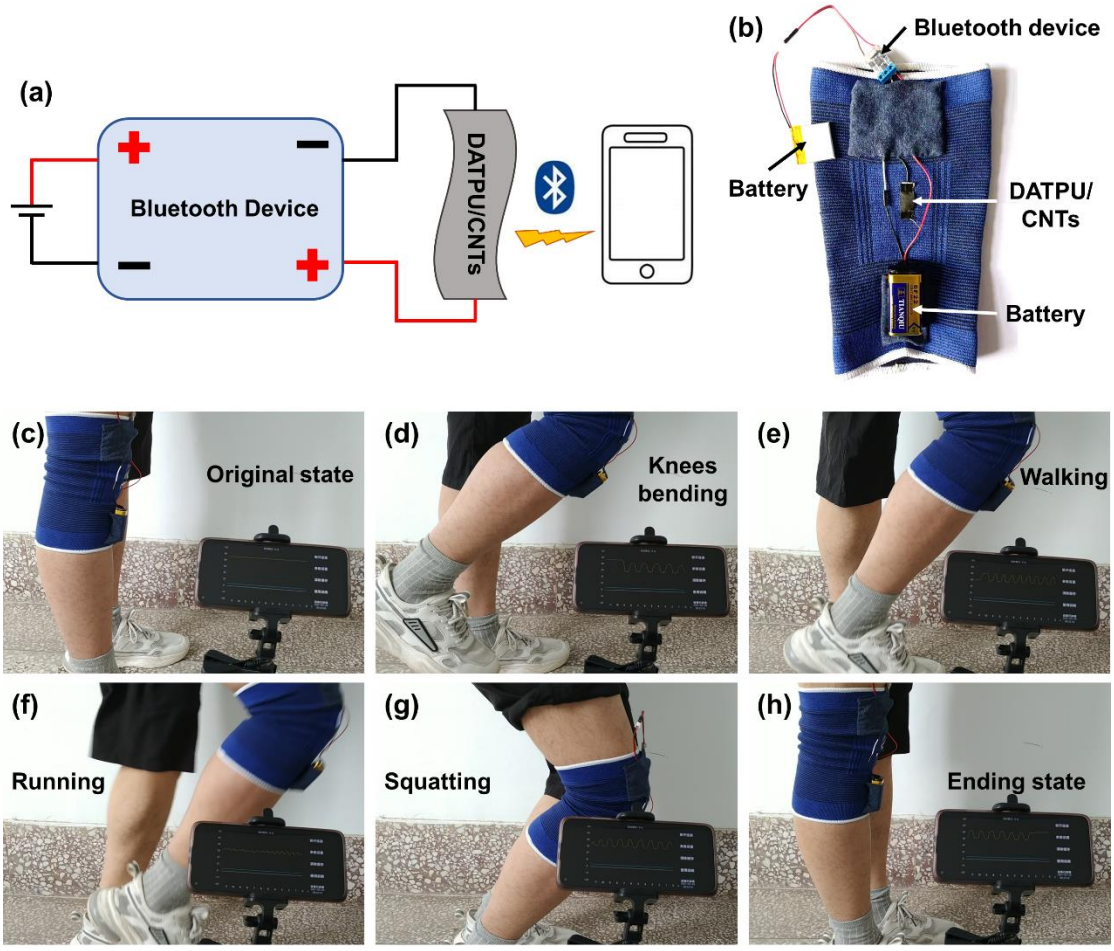

Figure 11 (a) diagram of main hardware circuit of the smart motion detection kneecap; (b) smart motion detection kneecap; detecting the human motion of (c) original state; (d) knees bending; (e) walking; (f) running; (g) squatting; (h) ending state using smart motion detection kneecap.

Conclusion

In this work, a strain sensor with ultra-high working range was fabricated by coating CNTs on the TPU electrospun fibrous membrane via ultrasonication. The amount and fastness of CNTs coated on the TPU fibrous membrane was enhanced by utilizing the rapid dopamine modification assisted with $NaIO_4$. As demonstrated in the results, DATPU/CNTs exhibited ultra-high working range of 710% with a good sensitivity of GF up to 1200. Due to the dopamine layer, DATPU/CNTs represented an excellent washing fastness. In addition, under different stretching rate and strain level, the DATPU/CNTs membrane displayed a good working stability. An excellent durability and a good reproducibility were observed during 15000 cycles of stretching-releasing test. Finally, DATPU/CNTs can accurately sense different degrees of human movement, such as finger bending, swallow, wrist bending and knee bending, indicating great promising for application in wearable devices.

Acknowledgment

The authors gratefully acknowledge the National Natural Science Foundation of China (Grant no. 51703108 and Grant no. 52003130), the Postdoctoral Science Foundation of China (Grant no. 2019M652318) and Taishan Scholar Foundation of Shandong, China (Grant no. tsqn201909100) for financial support.

References

[1] Z. He, G. Zhou, J.-H. Byun, S.-K. Lee, M.-K. Um, B. Park, T. Kim, S.B. Lee, T.-W.

Chou, Highly stretchable multi-walled carbon nanotube/thermoplastic polyurethane composite fibers for ultrasensitive, wearable strain sensors, Nanoscale, 11 (2019) 5884-5890.

[2] G. Zhou, J.-H. Byun, Y. Oh, B.-M. Jung, H.-J. Cha, D.-G. Seong, M.-K. Um, S. Hyun, T.-W. Chou, Highly sensitive wearable textile-based humidity sensor made of high-strength, single-walled carbon nanotube/poly (vinyl alcohol) filaments, ACS applied materials & interfaces, 9 (2017) 4788-4797.

[3] B. Zhou, Z. Liu, C. Li, M. Liu, L. Jiang, Y. Zhou, F.L. Zhou, S. Chen, S. Jerrams, J. Yu, A Highly Stretchable and Sensitive Strain Sensor Based on Dopamine Modified Electrospun SEBS Fibers and MWCNTs with Carboxylation, Advanced Electronic Materials, (2021) 2100233.

[4] Y. Ma, N. Liu, L. Li, X. Hu, Z. Zou, J. Wang, S. Luo, Y. Gao, A highly flexible and sensitive piezoresistive sensor based on MXene with greatly changed interlayer distances, Nature communications, 8 (2017) 1-8.

[5] J. Di, X. Zhang, Z. Yong, Y. Zhang, D. Li, R. Li, Q. Li, Carbon‐nanotube fibers for wearable devices and smart textiles, Advanced materials, 28 (2016) 10529-10538.

[6] C. Yan, J. Wang, W. Kang, M. Cui, X. Wang, C.Y. Foo, K.J. Chee, P.S. Lee, Highly stretchable piezoresistive graphene–nanocellulose nanopaper for strain sensors, Advanced materials, 26 (2014) 2022-2027.

[7] L. Jiang, Y. Wang, X. Wang, F. Ning, S. Wen, Y. Zhou, S. Chen, A. Betts, S. Jerrams, F.-L. Zhou, Electrohydrodynamic printing of a dielectric elastomer actuator and its application in tunable lenses, Composites Part A: Applied Science and Manufacturing,

147 (2021) 106461.

[8] S. Seyedin, P. Zhang, M. Naebe, S. Qin, J. Chen, X. Wang, J.M. Razal, Textile strain sensors: a review of the fabrication technologies, performance evaluation and applications, Materials Horizons, 6 (2019) 219-249.

[9] Y. Zhao, M. Ren, Y. Shang, J. Li, S. Wang, W. Zhai, G. Zheng, K. Dai, C. Liu, C. Shen, Ultra-sensitive and durable strain sensor with sandwich structure and excellent anti-interference ability for wearable electronic skins, Composites Science and Technology, 200 (2020) 108448.

[10] X. Fu, M. Ramos, A.M. Al-Jumaily, A. Meshkinzar, X. Huang, Stretchable strain sensor facilely fabricated based on multi-wall carbon nanotube composites with excellent performance, Journal of Materials Science, 54 (2019) 2170-2180.

[11] Y. Li, B. Zhou, G. Zheng, X. Liu, T. Li, C. Yan, C. Cheng, K. Dai, C. Liu, C. Shen, Continuously prepared highly conductive and stretchable SWNT/MWNT synergistically composited electrospun thermoplastic polyurethane yarns for wearable sensing, Journal of Materials Chemistry C, 6 (2018) 2258-2269.

[12] T. Yan, Z. Wang, Z.-J. Pan, Flexible strain sensors fabricated using carbon-based nanomaterials: A review, Current Opinion in Solid State and Materials Science, 22 (2018) 213-228.

[13] S. Gong, D.T. Lai, B. Su, K.J. Si, Z. Ma, L.W. Yap, P. Guo, W. Cheng, Highly stretchy black gold E‐Skin nanopatches as highly sensitive wearable biomedical sensors, Advanced Electronic Materials, 1 (2015) 1400063.

[14] X. Yue, Y. Jia, X. Wang, K. Zhou, W. Zhai, G. Zheng, K. Dai, L. Mi, C. Liu, C.

Shen, Highly stretchable and durable fiber-shaped strain sensor with porous core-sheath structure for human motion monitoring, Composites Science and Technology, 189 (2020) 108038.

[15] T. Huang, P. He, R. Wang, S. Yang, J. Sun, X. Xie, G. Ding, Porous fibers composed of polymer nanoball decorated graphene for wearable and highly sensitive strain sensors, Advanced Functional Materials, 29 (2019) 1903732.

[16] L. Tong, X.X. Wang, X.X. He, G.D. Nie, J. Zhang, B. Zhang, W.Z. Guo, Y.Z. Long, Electrically Conductive TPU Nanofibrous Composite with High Stretchability for Flexible Strain Sensor, Nanoscale Research Letters, 13 (2018) 86.

[17] Y. Wang, W. Li, Y. Zhou, L. Jiang, J. Ma, S. Chen, S. Jerrams, F. Zhou, Fabrication of high-performance wearable strain sensors by using CNTs-coated electrospun polyurethane nanofibers, Journal of Materials Science, 55 (2020) 12592-12606.

[18] M. Amjadi, Y.J. Yoon, I. Park, Ultra-stretchable and skin-mountable strain sensors using carbon nanotubes–Ecoflex nanocomposites, Nanotechnology, 26 (2015) 375501.

[19] W. Li, Y. Zhou, Y. Wang, L. Jiang, J. Ma, S. Chen, F.L. Zhou, Core–Sheath Fiber‐Based Wearable Strain Sensor with High Stretchability and Sensitivity for Detecting Human Motion, Advanced Electronic Materials, 7 (2021) 2000865.

[20] W. Li, Y. Zhou, Y. Wang, Y. Li, L. Jiang, J. Ma, S. Chen, Highly Stretchable and Sensitive SBS/Graphene Composite Fiber for Strain Sensors, Macromolecular Materials and Engineering, 305 (2020) 1900736.

[21] J.R. Bautista-Quijano, P. Pötschke, H. Brünig, G. Heinrich, Strain sensing, electrical and mechanical properties of polycarbonate/multiwall carbon nanotube

monofilament fibers fabricated by melt spinning, Polymer, 82 (2016) 181-189.

[22] M. Cai, H. He, X. Zhang, X. Yan, J. Li, F. Chen, D. Yuan, X. Ning, Efficient Synthesis of PVDF/PI Side-by-Side Bicomponent Nanofiber Membrane with Enhanced Mechanical Strength and Good Thermal Stability, Nanomaterials, 9 (2018) 39.

[23] Y. Liu, H. Zheng, M. Liu, High performance strain sensors based on chitosan/carbon black composite sponges, Materials & Design, 141 (2017) 276-285.

[24] G. Li, K. Dai, M. Ren, Y. Wang, G. Zheng, C. Liu, C. Shen, Aligned flexible conductive fibrous networks for highly sensitive, ultrastretchable and wearable strain sensors, Journal of Materials Chemistry C, 6 (2018) 6575-6583.

[25] P. Costa, M.F. Carvalho, V. Correia, J.C. Viana, S. Lanceros-Méndez, Polymer Nanocomposite-Based Strain Sensors with Tailored Processability and Improved Device Integration, ACS Applied Nano Materials, 1 (2018) 3015-3025.

[26] L. Lu, X. Wei, Z. Ye, G. Zheng, K. Dai, C. Liu, C. Shen, A flexible and self-formed sandwich structure strain sensor based on AgNW decorated electrospun fibrous mats with excellent sensing capability and good oxidation inhibition properties, Journal of Materials Chemistry C, 5 (2017) 7035-7042.

[27] H. Gong, C. Cai, H. Gu, Q. Jiang, D. Zhang, Z. Cheng, Flexible and wearable strain sensor based on electrospun carbon sponge/polydimethylsiloxane composite for human motion detection, RSC Advances, 11 (2021) 4186-4193.

[28] M. Ren, Y. Zhou, Y. Wang, G. Zheng, K. Dai, C. Liu, C. Shen, Highly stretchable and durable strain sensor based on carbon nanotubes decorated thermoplastic polyurethane fibrous network with aligned wave-like structure, Chemical Engineering

Journal, 360 (2019) 762-777.

[29] R. Wang, N. Jiang, J. Su, Q. Yin, Y. Zhang, Z. Liu, H. Lin, F.A. Moura, N. Yuan, S. Roth, A Bi‐Sheath Fiber Sensor for Giant Tensile and Torsional Displacements, Advanced Functional Materials, 27 (2017) 1702134.

[30] W. Zeng, L. Shu, Q. Li, S. Chen, F. Wang, X.M. Tao, Fiber‐based wearable electronics: a review of materials, fabrication, devices, and applications, Advanced materials, 26 (2014) 5310-5336.

[31] M. Xu, J. Qi, F. Li, Y. Zhang, Highly stretchable strain sensors with reduced graphene oxide sensing liquids for wearable electronics, Nanoscale, 10 (2018) 5264-5271.

[32] Z. Cui, J. Lin, C. Zhan, J. Wu, S. Shen, J. Si, Q. Wang, Biomimetic composite scaffolds based on surface modification of polydopamine on ultrasonication induced cellulose nanofibrils (CNF) adsorbing onto electrospun thermoplastic polyurethane (TPU) nanofibers, Journal of Biomaterials Science, Polymer Edition, 31 (2020) 561-577.

[33] P. Alves, S. Pinto, H.C. de Sousa, M.H. Gil, Surface modification of a thermoplastic polyurethane by low‐pressure plasma treatment to improve hydrophilicity, Journal of Applied Polymer Science, 122 (2011) 2302-2308.

[34] L. Shanmugam, X. Feng, J. Yang, Enhanced interphase between thermoplastic matrix and UHMWPE fiber sized with CNT-modified polydopamine coating, Composites Science and Technology, 174 (2019) 212-220.

[35] S. Liu, C.-M. Chan, L.-T. Weng, L. Li, M. Jiang, Surface Characterization of Poly

(styrene-co-p-hexafluoro-hydroxyisopropyl-α-methylstyrene)/Poly (4-vinylpyridine) Blends Spanning the Immiscibility− Miscibility− Complexation Transition by XPS, ToF-SIMS, and AFM, Macromolecules, 35 (2002) 5623-5629.

[36] H. Bi, Y. Li, S. Liu, P. Guo, Z. Wei, C. Lv, J. Zhang, X. Zhao, Carbon-nanotube-modified glassy carbon electrode for simultaneous determination of dopamine, ascorbic acid and uric acid: The effect of functional groups, Sensors and Actuators B: Chemical, 171 (2012) 1132-1140.

[37] J. Gao, W. Li, H. Shi, M. Hu, R.K.Y. Li, Preparation, morphology, and mechanical properties of carbon nanotube anchored polymer nanofiber composite, Composites Science and Technology, 92 (2014) 95-102.

[38] J. Lin, W. Wang, J. Cheng, Z. Cui, J. Si, Q. Wang, W. Chen, Modification of thermoplastic polyurethane nanofiber membranes by in situ polydopamine coating for tissue engineering, Journal of Applied Polymer Science, 137 (2020) 49252.

[39] C. Lee, L. Jug, E. Meng, High strain biocompatible polydimethylsiloxane-based conductive graphene and multiwalled carbon nanotube nanocomposite strain sensors, Applied Physics Letters, 102 (2013) 183511.

[40] J. Zhao, C. He, R. Yang, Z. Shi, M. Cheng, W. Yang, G. Xie, D. Wang, D. Shi, G. Zhang, Ultra-sensitive strain sensors based on piezoresistive nanographene films, Applied Physics Letters, 101 (2012) 063112.

[41] X.W. Zhang, Y. Pan, Q. Zheng, X.S. Yi, Time dependence of piezoresistance for the conductor‐filled polymer composites, Journal of Polymer Science part B: polymer physics, 38 (2000) 2739-2749.

[42] J.G. Simmons, Generalized formula for the electric tunnel effect between similar electrodes separated by a thin insulating film, Journal of applied physics, 34 (1963) 1793-1803.

[43] P. Sheng, E. Sichel, J.I. Gittleman, Fluctuation-induced tunneling conduction in carbon-polyvinylchloride composites, Physical Review Letters, 40 (1978) 1197.

[44] K. Yang, F. Yin, D. Xia, H. Peng, W. Yuan, A highly flexible and multifunctional strain sensor based on a network-structured MXene/polyurethane mat with ultra-high sensitivity and a broad sensing range, Nanoscale, 11 (2019) 9949-9957.

[45] X. Wang, S. Meng, M. Tebyetekerwa, Y. Li, J. Pionteck, B. Sun, Z. Qin, M. Zhu, Highly sensitive and stretchable piezoresistive strain sensor based on conductive poly (styrene-butadiene-styrene)/few layer graphene composite fiber, Composites Part A: Applied Science and Manufacturing, 105 (2018) 291-299.

[46] Y. Zhou, P. Zhan, M. Ren, G. Zheng, K. Dai, L. Mi, C. Liu, C. Shen, Significant stretchability enhancement of a crack-based strain sensor combined with high sensitivity and superior durability for motion monitoring, ACS applied materials & interfaces, 11 (2019) 7405-7414.

[47] X. Wang, H. Sun, X. Yue, Y. Yu, G. Zheng, K. Dai, C. Liu, C. Shen, A highly stretchable carbon nanotubes/thermoplastic polyurethane fiber-shaped strain sensor with porous structure for human motion monitoring, Composites Science and Technology, 168 (2018) 126-132.

[48] H. Wu, Q. Liu, H. Chen, G. Shi, C. Li, Fibrous Strain Sensor with Ultra-sensitivity, Wide Sensing Range, and Large Linearity for Full-Range Detection of Human Motion,

Nanoscale, 10 (2018) 1-9.

[49] X. Wang, X. Liu, D.W. Schubert, Highly sensitive ultrathin flexible thermoplastic polyurethane/carbon black fibrous film strain sensor with adjustable scaffold networks, Nano-Micro Letters, 13 (2021) 1-19.

[50] S. Ribeiro, P. Costa, C. Ribeiro, V. Sencadas, G. Botelho, S. Lanceros-Méndez, Electrospun styrene–butadiene–styrene elastomer copolymers for tissue engineering applications: Effect of butadiene/styrene ratio, block structure, hydrogenation and carbon nanotube loading on physical properties and cytotoxicity, Composites Part B: Engineering, 67 (2014) 30-38.

[51] S. Cantournet, R. Desmorat, J. Besson, Mullins effect and cyclic stress softening of filled elastomers by internal sliding and friction thermodynamics model, International Journal of Solids and Structures, 46 (2009) 2255-2264.

Video

Click here to access/download

Video

Movie S1.mp4

Click here to access/download

Video

Movie S2.mp4